



A predictive modelling strategy for warpage and shrinkage defects in plastic injection molding using fuzzy logic and pattern search optimization

Steven O. Otieno¹ · Job M. Wambua² · Fredrick M. Mwema^{2,3}  · Edwell T. Mharakurwa¹ · Tien-Chien Jen³ · Esther T. Akinlabi²

Received: 8 October 2023 / Accepted: 13 January 2024

© The Author(s), under exclusive licence to Springer Science+Business Media, LLC, part of Springer Nature 2024

Abstract

Quality control through defect minimization has been the central theme in plastic injection molding research. This study contributes to this course through the introduction of an alternative predictive modelling strategy for injection molding defects. Through multi-stage design of experiments, Computer Aided Engineering simulations, and intelligent algorithms, the study developed a warpage and shrinkage defects predictive model based on processing parameters. In the factorial design of experiment stage, the main effect sizes, interaction effect sizes, and ANOVA were used for process parameter screening. Next, a Taguchi L25 design was used for the generation of predictive model training data. Fuzzy logic models were then developed to predict warpage and shrinkage defects based on given process parameters and the predictive capability of triangular and Gaussian membership functions was investigated. A pattern search algorithm was utilized to tune the developed predictive models. The resulting predictive model had root mean square error (RMSE) of 0.04, standard error of regression (S) of 9.6, and coefficient of determination (R^2) of 98.7% for shrinkage prediction. The respective model metrics for warpage prediction were 0.005, 1.2, and 96.3%. The triangular membership function model had lower RMSE indicating a higher predictive accuracy whereas the Gaussian membership function model had lower S indicating a higher model reliability. Tuning of the predictive models using a pattern search algorithm reduced the RMSE and S and increased the models' R^2 . The approach can be adopted by plastic processing industries to predict and control such (and related) defects for quality products and maximum productivity.

Keywords Injection molding · Warpage and shrinkage · Predictive model · Fuzzy logic · Pattern search · Interaction effect

Introduction

Plastic injection molding (PIM) is one of the most widely used plastic manufacturing methods due to its ability to form complex and geometrically accurate parts on a large scale. It has since been of great interest globally with several researches carried out in attempts to optimize and improve the performance of the production process, technology, and equipment involved. Owing to vast areas of application for

plastic injection molded products, quality control has become an essential aspect of the plastic injection molding process (Chen & Turng, 2005). Shrinkage and warpage defects are among the major defects in plastic injection molded products which largely affect the performance, aesthetic appearance, and assembly of the plastic part components (Zhao et al., 2022). Major strategies for the reduction of shrinkage and warpage defects in plastic injection molded parts involve the selection of polymer material with suitable properties (Huszar et al., 2015), part geometry design (Fischer, 2013), injection mold design (Fu & Ma, 2016) and optimization of process parameters (Mohan et al., 2017). Of these methods, material selection, part geometry design, and mold design are normally determined at the initial design stages and may not be subject to changes. However, process parameters such as temperatures and pressures are normally dynamic in most

✉ Fredrick M. Mwema
fredrick.mwema@northumbria.ac.uk

¹ Dedan Kimathi University of Technology, Nyeri, Kenya

² Northumbria University, Newcastle, UK

³ University of Johannesburg, Johannesburg, South Africa

molding environments and may be subjected to changes as a result of influences from environmental conditions (Fischer, 2013).

Despite greater efforts to minimize shrinkage and warpage in plastic injection molded products through optimization of process parameters, the defects still exist as a result of interference of the molding process with several related and independent process parameters (Zhao et al., 2022). The complexity and non-linearity between the process variables and quality indices have resulted in the use of advanced data-driven models for process modeling and optimization (Rosato & Rosato, 2012). Artificial intelligence has emerged as a powerful tool and revolutionized quality control in the plastic injection molding process in terms of defect prediction. Case based reasoning is one of the many artificial intelligence technologies utilized for injection molding process parameter setting and has been adopted by many studies owing to its high retrieval accuracy and sensitivity (Khosravi & Nasiri, 2020; Yu et al., 2022). Moreover, Silva et al. (2023) introduced a real-time data collection and process classification methodology based on a zero-defect manufacturing platform. Through predictive modelling based on Artificial Neural Networks, the authors managed to both monitor the injection molding process deviations and predict molded part defects. This resulted to an improvement in the injection molding machine overall equipment effectiveness, a reduction in machine downtime, and a reduction in non-conforming parts thereby contributing to sustainable production through zero-defect manufacturing. Based on the positive results and insights obtained by Silva et al. (2023), data-based defect predictive modelling is a good way to accelerate the use of artificial intelligence for injection molding process improvement and hence is the main context of this study. Modelling and optimization of the injection molding process through the use of artificial intelligent algorithms is thus a theme of current studies and provides a yardstick for quality control.

Through the integration of design of experiments (DOE), Computer Aided Engineering (CAE) numerical simulations, and intelligent algorithms, warpage and shrinkage defects in injection molded parts have been predicted and controlled. CAE modelling has revolutionized manufacturing processes as it has enabled designers and engineers to simulate, analyze, and optimize various aspects of the product manufacturing process. It has become an indispensable part of modern manufacturing and has driven advancements in major fields such as plastic processing (Zhou, 2013), machining (López De Lacalle et al., 2005), and welding (Ai et al., 2023a, 2023b; Ai et al., 2023a, 2023b). The utilization of CAE modelling for manufacturing process improvement has been recommended by several studies such as Lopez De Lacalle et al. (2005) among other earlier visionary works. In their work, they introduced the concept of the use of virtual machining simulation

utility during a milling program preparation stage for an optimum cutting force and a collision-free tool-path. Remarkable results obtained from the study with respect to significant reduction in defective machined parts and 20% reduction in machining time positions CAE as the center of manufacturing thereby inspiring subsequent studies such as this study on the applications of various aspects of computer aided engineering to manufacturing. Numerical simulations through CAE have thus become popular, especially for simulating the occurrence of defects such as shrinkage and warpage which have proven difficult to measure and quantify experimentally.

Yin et al. (2011) developed a back propagation neural network model for predicting and optimizing warpage in an injection molded part. The study utilized CAE analysis data to train the neural network model. Song et al. (2020) presented a warpage and shrinkage predictive modelling strategy using CAE, neural networks, and genetic algorithms. The authors compared the predictive capabilities of Neural Networks, backpropagation genetic algorithms, and support vector algorithms thereby establishing that support vector-based model predictive capability was high with higher accuracy. Chen et al., (2023a, 2023b) carried out optimization and predictive modelling of warpage using statistical analysis. The study obtained warpage data through CAE simulations and developed a warpage predictive model using linear regression. A study by Li et al. (2019) developed three predictive models based on the response surface model to map relationships between various design parameters and three quality indices such as warpage, volumetric shrinkage, and residual stress. Ahmed et al. (2022) proposed a warpage prediction method using ensemble machine learning and compared the predictive capabilities of random forest and gradient-boosted predictive models. The study established that the random forest algorithm performed better than gradient gradient-boosted model for warpage prediction. Similarly, Abdul et al. (2019) and Altan (2010) developed shrinkage predictive models using a hybrid Taguchi and Artificial Neural Networks. The studies used experimental data to train the predictive models. Chen et al. (2020) developed an experimental on-line dimensional variation detection system based on multilinear regression and artificial neural network models and established that neural networks performed better than multilinear regression in defect detection. Using Taguchi DOE and CAE, Kumar et al. (2020) developed a warpage and shrinkage defects prediction model based on linear regression and utilized a particle swarm algorithm to optimize the developed predictive model. Wang et al. (2015) carried out warpage optimization using a Kriging model which was used to formulate a functional relationship between the maximum warpage objective and selected process parameters. Moreover, Gao and Wang (2008) used the Kriging model to optimize process parameters to reduce warpage in plastic injection molded product and the result

from the study showed a significant reduction in warpage with the utilization of the Kriging model algorithm. Therefore, of the majorly used intelligent models in predictive modelling of warpage and shrinkage defects, the use of artificial neural networks stands out both in process parameter optimization and quality prediction while other models such as genetic algorithms, Kriging model, particle swarm, and other hybrid models are majorly used for optimization.

Although significant strides have been made in literature about warpage and shrinkage defects predictive modelling, most studies have utilized a single-stage DOE for obtaining the model training data. Other studies that carried out process parameter screening concentrated on the parameters' mains effects only during the screening stage (Tsai & Luo, 2017). However, with the non-linear feature of the PIM process coupled with complex process parameter interactions, there is a need to explore multi-stage DOEs to enhance a thorough parameter space exploration during the screening stage and establish both the mains effect and critical interactions between process parameters and their effects to warpage and shrinkage defects. This way the most influential parameters could be identified and used for model development. Studies report that parameter screening without consideration of interactions for some complex systems may result in chances of wrong statistical inference, missing out on important parameters, and biased predictive estimates (Phoa et al., 2009). The first contribution of this study is that, contrary to the previous studies, this study considers parameter interaction effect sizes alongside the mains effects during the process parameter screening stage. That is, the selection of significant process parameters to be used for predictive model development has been guided by significant mains effects as well as interaction effects to enhance a robust model that incorporates the complex relationships among process parameters. Previous related defects predictive modelling studies have been based on single-stage designs of experiments with unclear parameter screening methods. Other studies that considered multi stage design of experiments carried out parameter screening based on mains effect only. Therefore, this study has shown that consideration of interaction effect sizes, which have not been considered in previous related studies, adds to the robustness and accuracy of predictive models.

In addition, various expert systems have been developed to aid in the prediction and control of warpage and shrinkage defects in the PIM process (Zhao et al., 2022). However, there is limited information in the literature regarding the application of fuzzy inference systems coupled with intelligent optimization algorithms in the prediction and control of these defects. The application of fuzzy inference systems to warpage and shrinkage predictive modelling could provide knowledge of the causal relationships among process parameters and the defects through the fuzzy rule interface.

This could provide more insight into the system and serve as a decision-support tool for effective monitoring and control. Moreover, previous studies have successfully explored applications of fuzzy logic models in the plastic injection molding process for purposes such as quality evaluation and process parameter optimization (Moayyedean et al., 2018) and barrel temperature control (Hu & Wu, 2022). Therefore, the second contribution of this study is that it introduces a warpage and shrinkage defects predictive modelling strategy using fuzzy logic integrated with a pattern search optimization algorithm. The utilization of fuzzy logic in defects predictive modelling has not been widely explored despite its strengths such as the incorporation of expertise in rule base generation and provision of transparent prediction. The study introduces the use of a pattern search algorithm to guide the machine learning process through tuning and has shown that the incorporation of conventional algorithms to predictive modelling enhances model performance. To the best of our knowledge, limited warpage and shrinkage predictive modelling studies have considered parameter interaction effect sizes during parameter screening and investigated the applicability of tuned fuzzy logic models for the defects prediction.

A two-stage DOE was used which involved a detailed mains and interaction effects analysis in the parameter screening stage and the incorporation of multiple parameter levels in the second DOE stage to enhance a more robust predictive model design. The results of this study provide an alternative warpage and shrinkage predictive modelling strategy and form a wider contribution toward effective defects control in the plastic injection molding process.

Method

This study used a combination of the design of experiment, CAE simulations, and intelligent algorithms for warpage and shrinkage defect modelling. In this research, the numerical data used for predictive model training and validation were obtained using Moldex3D® R22 CAE software and the fuzzy predictive model developed and tuned using MATLAB® Fuzzy Logic Designer Toolbox. The three main phases of the study included finite element model development for CAE simulations, design of experiments and numerical simulations for data collection and predictive model development. Figure 1 illustrates the methodology used for the study. Upon the development of a two-cavity injection mold as a finite element model, the model was verified through a comparison of numerical density computations with analytical computations at the same process parameters. Numerically obtained data was validated through comparison of mains effect trends with experimental mains effect trends reported in the literature.

Fig. 1 Study design

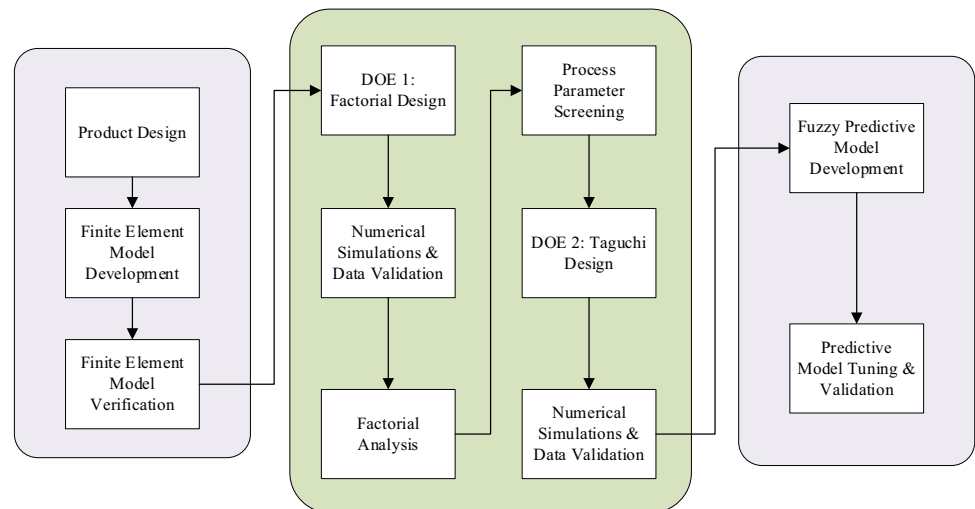


Table 1 Polymer material properties

Family name	HDPE
Grade name	HDPE 2001 PBK44
Producer	Total chemicals
Processing Temperatures	190–250 °C
Solid density	0.954 g/cm ³
Yield strength	24 MPa
Flexural modulus	1.0GPa
Poisson's ration	0.4

Finite element modelling

Finite element model development

In this study, a two-cavity injection mold for making a standard-size packaging bottle cap was developed as a finite element model used for injection molding process modelling through numerical simulations. A bottle cap was selected for this study due to its complex shape of regions with varying wall thickness, ribs and provisions for undercuts. The largest product diameter was 30 mm, longest height of 12 mm with a maximum thickness of 2.03 mm and a minimum thickness being 0.03 mm. The selected cap product material for this study was a commercially available grade of high-density polyethylene produced by Total Chemicals under the commercial name HDPE 2001 PBK44. This material is commonly used for making plastic packaging products and some of its major properties are highlighted in Table 1 based on Moldex3D Material Library.

Injection mold modelling entailed the definition and sizing of the core and cavity plates, feed system and cooling system. Feed system design involved the specification of features such as gates, runners and sprue which achieves the objective

of conveyance of the polymer melt from a molding machine nozzle to the cavities. This study adopted a 5-layer boundary layer mesh configuration as used by Zhang et al. (2019) who established a good qualitative consistency between simulation and experimental results. Figure 2 shows the part 5-layer boundary layer mesh configuration used for the part. The configuration shows a tetra layer sandwiched between two 5-layer boundary layers.

Surface mesh was generated for the part while solid mesh was generated for the part, feed system, cooling system and mold base. Different forms of surface mesh node seeding and solid mesh were applied to the part, feed system, cooling system and mold base depending on the criticality and contribution of the section for the analysis. Figure 3 shows the finite element model of the injection mold components. Node seeding and specification of the surface mesh size were modified around the mold base, part edges and for sections of the part with critical features such as the lower regions with thinner wall sections. Tetrahedral mesh elements with four computational nodes were used in the tetrahedral layer while prismatic elements with six computational nodes were used in the boundary layers. For curve meshing, hexahedral-type mesh with five inner layers and five outer layers was used for the feed system and cooling system. Tetrahedral mesh element type was used for the mold base solid mesh due to their flexibility and efficiency in capturing heat transfer which is the sole contribution of the mold base in analyses.

To determine the best mesh size for the analysis, a mesh convergence test was carried out to determine the extent of the effects of variation in mesh sizes to warpage (Yang et al., 2022). Warp simulations were carried out while refining the mesh properties from a default size of 2 mm to 0.2 mm. Figure 4 shows the results of the systematic mesh refinement process indicating the maximum total displacement obtained

Fig. 2 Sectional view of the part showing a 5-layer boundary layer mesh configuration

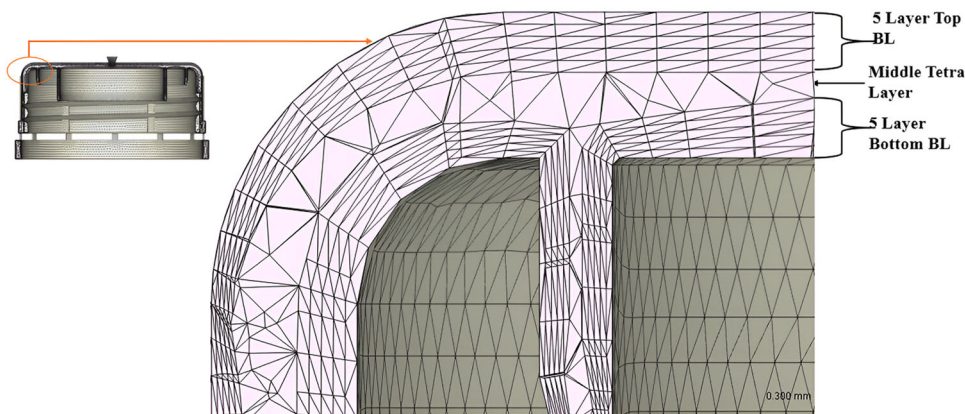


Fig. 3 Finite Element Model of the mold

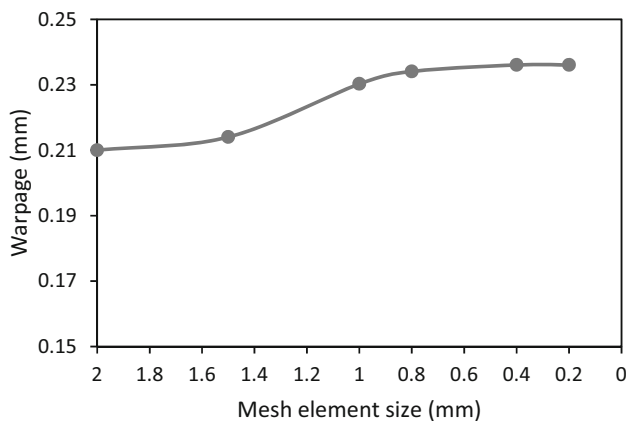
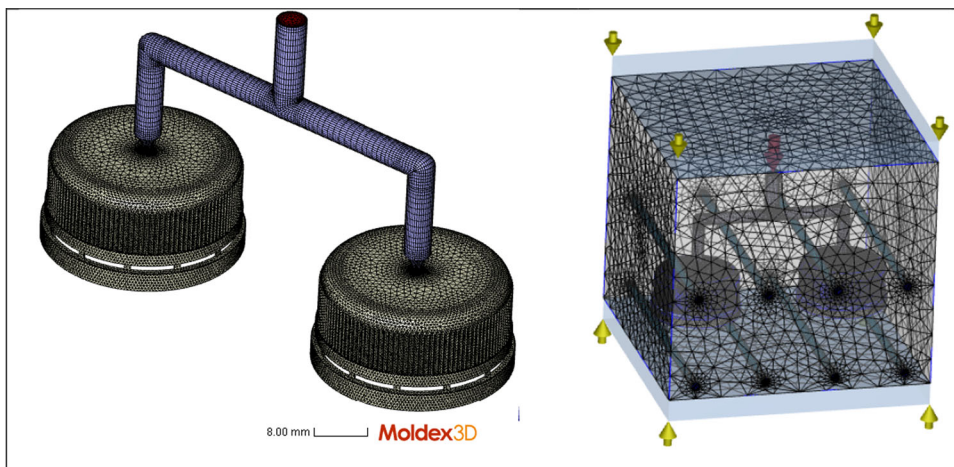


Fig. 4 Systematic mesh refinement results showing the variation of warpage with mesh size

at the various mesh element sizes. The figure shows significant changes in part warpage with a reduction of mesh size from 2 mm to 0.4 mm. Beyond 0.4 mm, a further reduction in mesh size would just increase the simulation time without significantly affecting the warpage result. A mesh size of 0.4 mm was thus used for the rest of the part, 0.2 mm

for lower regions of the part with thinner cross sections at a boundary layer offset ratio of 1.

Governing equations

Numerical analysis was based on the flow of the polymer as governed by Eqs. 1, 2 and 3 derived from the principles of conservation of mass, energy and momentum respectively (Kennedy & Zheng, 2013).

$$\frac{D\rho}{Dt} = -\rho \nabla \cdot u \quad (1)$$

$$\rho \frac{\partial v}{\partial t} = \rho g - \nabla p + \nabla \cdot \eta D - \rho v \cdot \nabla v \quad (2)$$

$$\rho C_p \left(\frac{\partial T}{\partial t} + v \cdot \nabla T \right) = \beta T \left(\frac{\partial P}{\partial t} + v \cdot \nabla P \right) + \eta \dot{\gamma}^2 + k \nabla^2 T \quad (3)$$

where ρ is the density, t is the time, u is the speed vector, v is the specific volume, g is the gravitational acceleration, P is the hydrostatic pressure, C_p is the specific heat, T is the temperature, β is the heat expansion coefficient, k is the thermal conductivity and $\dot{\gamma}$ is the shear rate. Viscosity of the polymer melt was modelled using modified cross exponential

viscosity model given by Eqs. 4 and 5 (Lin et al., 2022).

$$\eta(\dot{\gamma}, T, P) = \frac{\eta_0(T, P)}{1 + \left(\frac{\eta_0 \dot{\gamma}}{\tau^*}\right)^{1-n}} \quad (4)$$

$$\eta_0(T, P) = B \exp\left(\frac{T_b}{T} + DP\right) \quad (5)$$

where η_0 is the zero shear viscosity, $\dot{\gamma}$ is the effective shear rate, τ^* is the reference shear stress, n is the power law index, P is the pressure T is the temperature and the other material constants given by B , D and T_b . The position of the polymer melt front during the molding process was determined based on a volume fraction function governed by the transport Eq. 6 (Yang et al., 2004).

$$\frac{\partial f}{\partial t} + \nabla \cdot (uf) = 0 \quad (6)$$

where;

$f = 0$ at the air phase, $f = 1$ at the polymer melt phase

$0 < f < 1$ at melt front location

Pressure Volume Temperature (PVT) behavior of the material during end of fill and packing phase was modelled using modified Tait Eq. 7 (Chang et al., 1996).

$$V(P, T) = V_0(T) \left[1 - C \cdot \ln \left(1 + \frac{P}{B(T)} \right) \right] + V_t(P, T) \quad (7)$$

where;

$$V_0(T) = \begin{cases} b_{1L} + b_{2L} \bar{T}, & T > T_t, \text{ meltstate} \\ b_{1s} + b_{2s} \bar{T}, & T \leq T_t, \text{ solidstate} \end{cases}$$

$$B(T) = \begin{cases} b_{3L} \exp(-b_{4L} \bar{T}), & T > T_t, \text{ meltstate} \\ b_{3s} \exp(-b_{4s} \bar{T}), & T \leq T_t, \text{ solidstate} \end{cases}$$

$$V_t(P, T) = \begin{cases} 0, & T > T_t, \text{ meltstate} \\ b_7 \exp(b_8 \bar{T} - b_9 P), & T \leq T_t, \text{ solidstate} \end{cases}$$

$$\bar{T} = T - b_5, T_t = b_5 + b_6 P$$

$b_{1L} = b_{1s}$ for amorphous polymers

$b_{1L} > b_{1s}$ for crystalline polymers

$$C = 0.0894$$

Standard three-dimensional residual stress models given by Eqs. 8 and 9 were used to model shrinkage and warpage

(Kennedy & Zheng, 2013).

$$\sigma = C(\varepsilon - \varepsilon^0 - \alpha \Delta T) \quad (8)$$

$$\varepsilon = \frac{1}{2} \left(\frac{\partial u_i}{\partial x_j} + \frac{\partial u_j}{\partial x_i} \right) \quad (9)$$

where σ is the stress tensor, C is the stiffness tensor, ε is the strain tensor, u is the displacement tensor and α is the CLET tensor.

Boundary and initial conditions were described by Eqs. 10, 11, 12, 13, 14 and 15 (Huszar et al., 2015).

$$\vec{u} = 0; T = T_w; \frac{\partial P}{\partial n} = 0 \text{ at } z = \pm h \text{ (at the cavity wall)} \quad (10)$$

$$\frac{\partial \vec{u}}{\partial z} = \frac{\partial T}{\partial z} = 0 \text{ at } z = 0 \text{ (at the centerline)} \quad (11)$$

$$P = 0 \text{ (at the flow front)} \quad (12)$$

$$P_{inlet} = P(x, y, z, t); T_{inlet} = T_{melt} \text{ (at the inlet)} \quad (13)$$

$$Time_{fill} = 0.13s \quad (14)$$

$$T_{eject} = 112.35^\circ C; T_{air} = 25^\circ C \text{ (at ejection)} \quad (15)$$

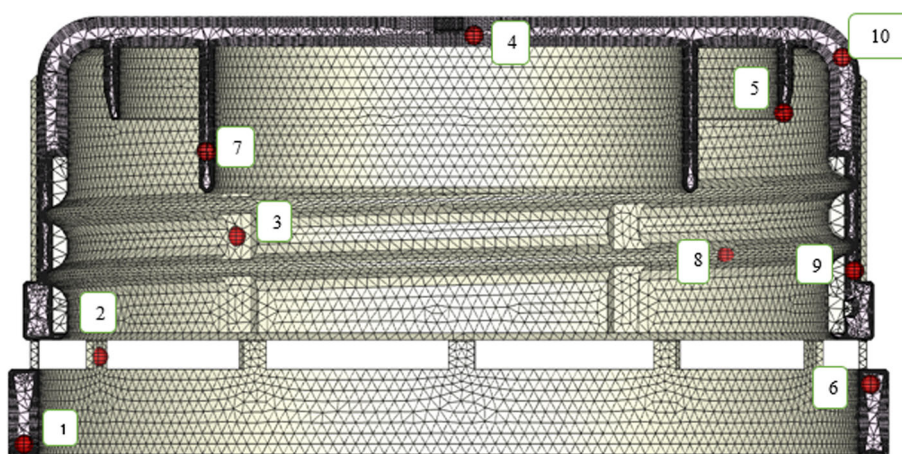
where u is the inlet velocity, T_w is mold temperature, P is pressure and t is time.

The model was based on assumptions such as the melt flow considered an extended laminar flow of incompressible fluid, inertial force ignored due to high viscosity, heat convection in the thickness direction ignored, heat conduction in the direction of melt flow lower than heat convection hence ignored and physical properties such as density and viscosity at any point in the fluid assumed to vary smoothly over space and time (Kennedy & Zheng, 2013). In this study, a numerical solver based on 3D Finite Element approximation was utilized due to its suitability to solve complex geometries or irregular shapes (Zhou, 2013), such as the one used in this study.

Finite Element model verification

To determine how well the calculations were implemented on the finite element model, the study verified the characterization of the pressure–volume–temperature (PVT) relationship which is important in the calculation of the material compressibility during the packing phase and final warpage and shrinkage phase upon ejection. This was achieved through a comparison of the numerical values of density obtained from a simulation run against those calculated from the analytical equations at the same conditions. Analytical solutions

Fig. 5 Section of the FE Model showing the positions of the probes at various nodes used to record the pressures, temperatures and densities in each node at EOF



of density were computed using modified Tait Eq. 7 which governs the change in specific volume of the polymer melt during the packing stage.

Ten probes were placed on various nodes of the part as shown in Fig. 5, a single warpage simulation run was made and parameters such as pressure, temperature and density were obtained from each node at the End of Fill (EOF). The densities obtained from each node at EOF represented numerically computed densities. Using pressure and temperature values obtained from each node, corresponding values of analytical densities were computed based on modified Tait Eq. 7 and the results were compared. For use with the modified Tait equation, material constants specific to Total 2001 PBK 44 HDPE material were obtained from the Moldex3D Warpage result log.

Figure 6 shows the comparative analytical and numerical density plots. Of the ten probes, the largest deviation between the analytical and numerical density was 0.0046 g/cm^3 which was deemed sufficient. These deviations were attributed to slight differences in underlying considerations during computations where analytical computations assumed steady-state conditions whereas numerical simulation took into account the transient behavior of the polymer material properties. The model therefore accurately predicted the changes in specific volume and hence the density of the polymer melt as a result of the changes in temperatures and pressures throughout the molding cycle. A match in the plots indicated an effective model characterization of the PVT relationship and suitability for PIM process modelling.

Design of experiments

Factorial experiment design

The selection of initial process parameters was made by examining related shrinkage and warpage defect optimization studies and associated significant process parameters

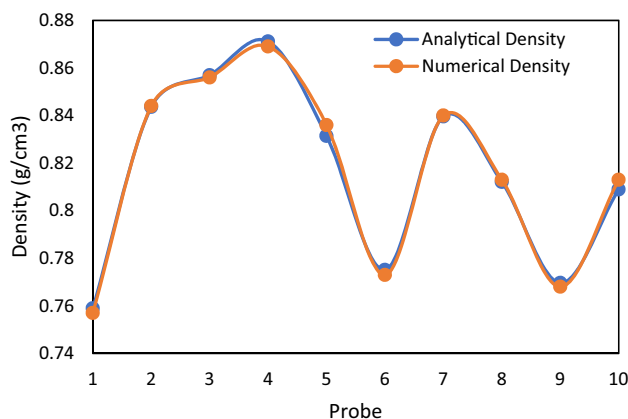


Fig. 6 Comparative density verification plots

Table 2 Selected factorial design process parameters and levels

Process parameters	Levels	
	Min	Max
Melt temperature (°C)	200	235
Mold temperature (°C)	30	50
Maximum injection pressure (MPa)	200	300
Maximum packing pressure (MPa)	200	300
Cooling time (s)	8	15
Packing time (s)	3	5

reported in various studies (Chen et al., 2023a, 2023b; Song et al., 2020). Six parameters including melt temperature, mold temperature, injection pressure, packing pressure, cooling time and packing time were found to be among the most significant and hence considered. For parameter screening through mains effects and lower order interaction effects, a half fractional factorial design of resolution VI was used (Packianather et al., 2013). Six parameters were used each at

two levels specific to Total 2001 PBK 44 HDPE material as illustrated in Table 2.

Numerical simulations were carried out at the given process parameter combinations to obtain the values of warpage and shrinkage responses. This was carried out through fill, pack, cool, and warp analyses. Table 3 shows the results obtained from numerical simulation. The maximum total warpage was obtained as the maximum total displacement given as a vector sum of the displacements along the x, y, and z axes of the part. Shrinkage was obtained as the maximum shrinkage of the part in the warpage phase of the analysis. Maximum warpage of 0.2373 mm obtained gave a warp ratio of 0.8% expressed as a percentage of the maximum part diameter and was above allowable warp ratio values of 0.2% to 0.5%.

Figure 7 shows the contour plots of the maximum values of warpage and shrinkage defects obtained. As shown on the plots, the regions of the part subjected to maximum warpage are subjected to average shrinkage whereas those regions subjected to maximum shrinkage have average warpage, an indication of the difference in terms of effects of process parameters to the two defects.

Numerical data validation

To determine whether the numerical results were an accurate prediction of a physical injection molding process, qualitative numerical data validation was done through a comparison of the data trends against those obtained experimentally and reported in the literature. Mains effect plots were made to represent the effects of the individual process parameters on the defects. Similarly, a mains effect plot was made for the experimental data published by Mukras et al. (2019). Similarity was obtained in the data trends as illustrated in Fig. 8 for A-Melt Temperature, B-Mold Temperature, C-Injection Pressure, D-Packing Pressure, E-Cooling Time and F-Packing Time. A general increase in melt temperature increased shrinkage whereas an increase in injection pressure, packing pressure, packing time and cooling time decreased shrinkage. Similar trends were reported by Abasalizadeh et al. (2018) who also carried out the study experimentally.

The simulation study yielded an increase in shrinkage with an increase in melt temperature which was the case in the experimental studies. This was as a result of the increase in molecular disintegration with an increase in melt temperature thereby increasing the rate of shrinkage. An increase in injection pressure ensures more material delivery and higher material compression inside the mold thereby lowering chances of volumetric shrinkage. An increase in packing time as well as packing pressure enhances an increase in material compensation within the mold thereby reducing shrinkage. An increase in cooling time ensures an increase

in stress relaxation time thereby reducing shrinkage (Abasalizadeh et al., 2018).

However, numerical data indicated a decrease in shrinkage with an increase in mold temperature while the experimental study reports an increase in shrinkage with increasing mold temperature. As reported by Mieth and Tromm (2016), mold temperature has an effect on shrinkage effects which could be either positive or negative. An increase in mold temperature could enhance polymer melt fluidity and increase flow into the cavity thereby reducing the chances of post-mold shrinkage. Conversely, an increase in mold temperature could also result in slower part cooling which would encourage a greater degree of crystallization thereby resulting to increased shrinkage (Fischer, 2013).

Factorial analysis

By substituting the lower parameter levels with -1 and higher levels with +1 and through a difference of means, the mains effect and interaction effect sizes were computed as the difference between average shrinkage and warpage responses at high (+) levels and low (-) levels of the effects.

Mains effect sizes are illustrated in Table 4. Packing pressure has the largest decreasing effect on both warpage and shrinkage defects. At high packing pressure, polymer chains are oriented in an organized manner and this orientation further reduces the internal stresses within the material and helps it maintain its shape and dimension. Apart from packing pressure, an increase in melt temperature decreases the warpage. Increasing the melt temperature ensures the material remains molten for a longer time during the cooling phase and thus undergoes a uniform solidification which minimizes the stresses that contribute to warpage. Similarly, a study by Chen and Zhu (2019), obtained a significant decrease in warpage at an increasing packing pressure and melt temperature.

Most process parameters were found to have a larger effect on shrinkage as compared to warpage. To visualize the extent of the effects of process parameters and their interactions on shrinkage, a Pareto plot was constructed as illustrated in Fig. 9. The largest interaction effect was a three-way interaction between melt temperature, mold temperature and injection pressure which was larger than the individual effects of the three parameters.

Also, many interactions with larger effects involved the melt temperature despite packing pressure being the parameter with the largest effect on shrinkage. This could be because the melt temperature setting influences the material viscosity, flow, and thermal behavior and therefore an interaction between the other process parameters and melt temperature would largely affect these properties and influence shrinkage.

Some of the major interaction effect sizes on shrinkage computed are given in Table 5. The combined effect of

Table 3 Numerical results showing warpage and shrinkage responses at various process parameter combinations

Run	Melt Temp. (°C)	Mold Temp. (°C)	Max Injection pressure (MPa)	Packing time (s)	Max packing pressure (MPa)	Cooling time (s)	Warpage (mm)	Shrinkage (%)
1	200	30	300	3	200	15	0.2372	1.44
2	235	50	200	3	300	15	0.1595	0.99
3	200	50	300	5	200	15	0.2373	1.23
4	200	30	300	5	200	8	0.2360	1.45
5	200	50	200	3	300	8	0.1778	1.33
6	235	50	200	5	300	8	0.1566	0.96
7	200	50	200	5	300	15	0.1784	0.57
8	200	30	300	5	300	15	0.1784	0.58
9	235	50	200	3	200	8	0.2226	1.94
10	235	30	300	3	200	8	0.2300	2.03
11	200	30	200	5	300	8	0.1782	0.98
12	200	30	200	3	200	8	0.2361	1.82
13	200	30	300	3	300	8	0.1782	1.33
14	235	30	200	3	200	15	0.2238	1.58
15	200	50	300	3	300	15	0.1785	0.99
16	200	50	300	5	300	8	0.1778	0.98
17	200	50	300	3	200	8	0.2363	1.81
18	200	30	200	5	200	15	0.2372	1.23
19	200	50	200	3	200	15	0.2373	1.43
20	200	50	200	5	200	8	0.2363	1.44
21	235	30	200	3	300	8	0.1557	1.39
22	235	50	200	5	200	15	0.2238	1.52
23	235	50	300	3	300	8	0.1566	1.35
24	235	30	300	5	200	15	0.2237	1.28
25	235	50	300	5	200	8	0.2225	1.50
26	235	30	300	5	300	8	0.1556	0.99
27	235	30	200	5	200	8	0.2227	1.54
28	200	30	200	3	300	15	0.1784	1.00
29	235	50	300	3	200	15	0.2238	1.52
30	235	50	300	5	300	15	0.1595	0.56
31	235	30	200	5	300	15	0.1590	0.58
32	235	30	300	3	300	15	0.1591	1.02

increasing the melt temperature (A), mold temperature (B) and injection pressure (C) reduces shrinkage by 0.076%. The interaction between these factors could affect material flow into a mold cavity. Higher melt temperature as well as mold temperature enhances smooth material flow into the cavities. A higher injection pressure then enhances the delivery of the smoothly flowing molten material to all sections of the cavity thus reducing the possibility of product shrinkage upon cooling and ejection.

A similar relationship was obtained between melt temperature and packing pressure (E) whose interaction equally

had a moderate contribution to shrinkage reduction. Individually, increasing melt temperature increases shrinkage while increasing packing pressure reduces shrinkage. When the two parameters are increased simultaneously, the shrinkage reduces but the extent of reduction depends on the levels of the parameters. At a melt temperature of 200 °C, an increase in packing pressure from 200 to 300 MPa would decrease shrinkage by 0.63% while at a melt temperature of 235 °C, the same amount of increase in packing pressure would decrease shrinkage by 0.51%.

Fig. 7 Contour plots showing the maximum values of warpage and shrinkage defects obtained

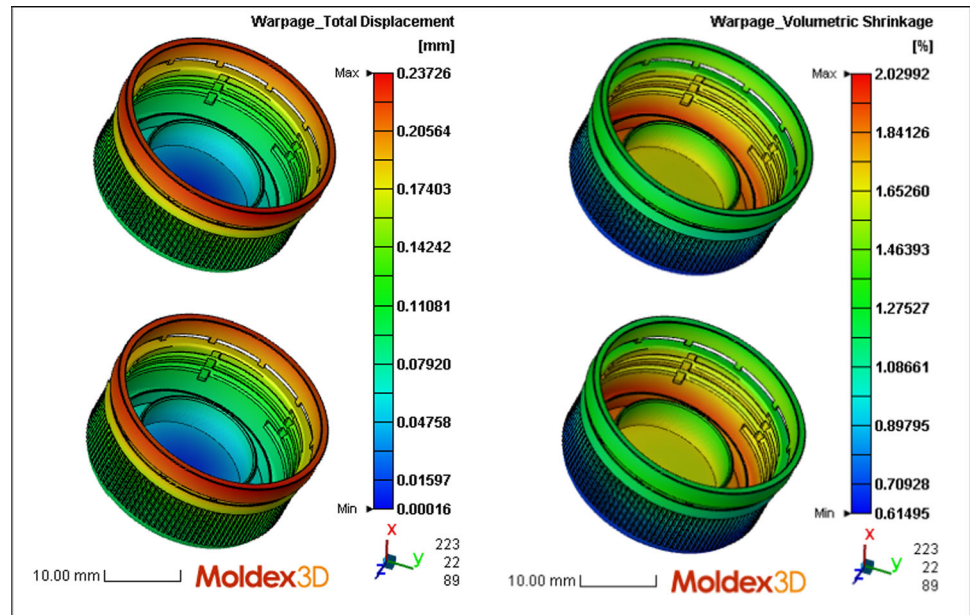


Fig. 8 Mains effect plots from numerical simulation and experiment showing the general comparative effects of the changes in process parameters to shrinkage

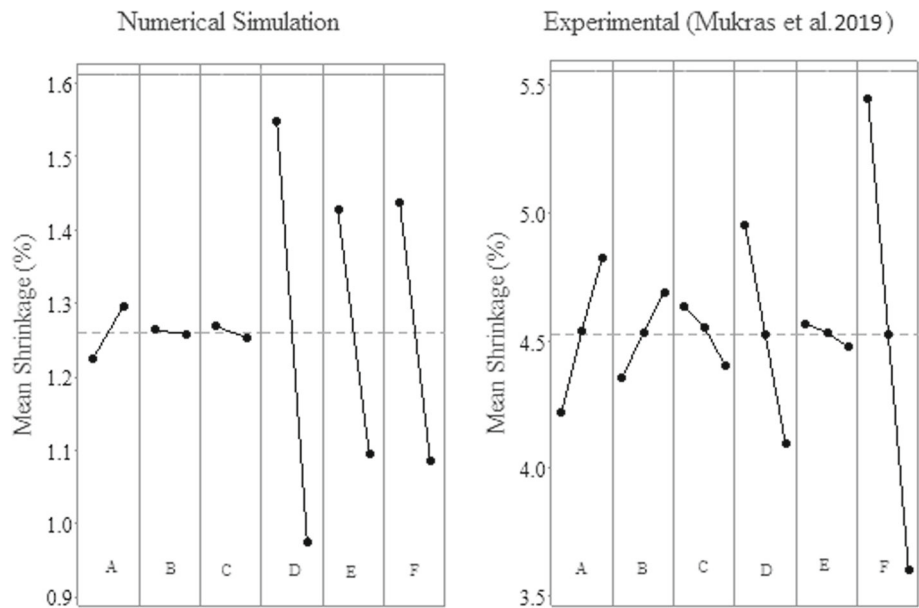


Table 4 Computed Mains Effect sizes

Defect	Melt Temp	Mold Temp	Injection pressure	Pack time	Pack pressure	Cool time
Warpage (mm)	- 0.017	1.5×10^{-4}	3.13×10^{-6}	$- 4.94 \times 10^{-5}$	- 0.062	0.001
Shrinkage (%)	0.071	- 0.005	- 0.015	- 0.350	- 0.572	- 0.331

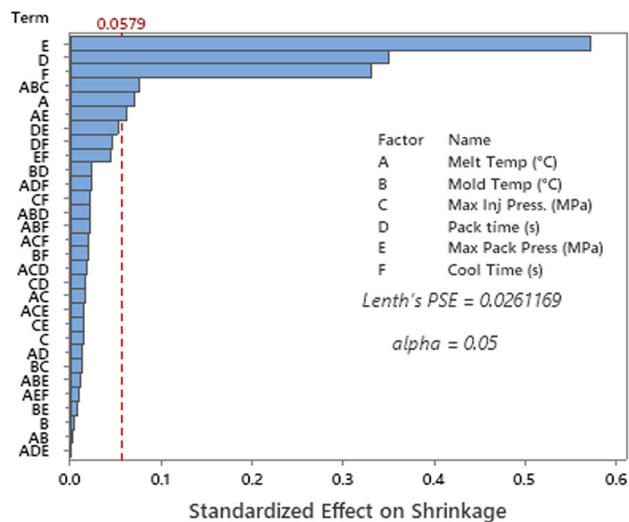


Fig. 9 Pareto chart of the effects of process parameters on shrinkage

Table 5 Interaction effect sizes on shrinkage

Parameter interaction	Effect on shrinkage (%)	Parameter interaction	Effect on shrinkage (%)
ABC	- 0.076	BD	0.023
AE	- 0.062	ADF	0.023
DE	- 0.053	CF	- 0.022
DF	0.047	ABD	0.022
EF	- 0.045	ABF	0.022

A combined effect of packing time and packing pressure on shrinkage was also imminent as a result of the contribution of the packing phase to shrinkage. Figure 10 shows a contour plot of packing pressure and time against shrinkage. A minimum shrinkage rate is obtained at higher packing pressure and packing time levels. At a low level of packing pressure, an increase in packing time decreases shrinkage by 0.3% whereas at a high level of packing pressure, the same increase in packing time decreases shrinkage by 0.4%.

For warpage defect, the largest interaction effect occurred between melt temperature and packing pressure. Higher values of warpage was obtained at lower values of packing pressure and melt temperatures while the lower warpage obtained at higher values of the two parameters as illustrated in Fig. 11. At lower packing pressure, an increase in melt temperature has a very minimal effect on the warpage whereas, at higher packing pressure, an increase in melt temperature substantially lowers the warpage. Conversely, increasing the packing pressure decreases warpage both at lower and higher levels of melt temperature with the largest decrease at higher melt temperature. Higher melt temperature lowers the material viscosity and increases its fluidity thereby enhancing

easier molecular orientation and reduction in internal stresses at higher packing pressure. Therefore, when all the other factors are held constant, warpage defect would be reduced significantly by raising the packing pressure at higher melt temperatures.

Process parameter screening

Selection of the most significant process parameters to be used for predictive model development was done based on the sizes of the mains effects and interaction effects results. ANOVA was carried out at a significance level of $\alpha = 0.05$ to verify the significance of computed effect sizes. Table 6 shows the ANOVA results of the warpage. ANOVA with main terms only yielded an R-squared of 99.67%, adjusted R-squared of 99.60% and predicted R-squared of 99.47% whereas ANOVA with interaction terms yielded an R-squared of 99.98%, adjusted R-squared of 99.96% and predicted R-squared of 99.91%. The increase in adjusted R-squared with the addition of interaction terms indicated that they improved the model and the smaller difference between R-squared and predicted R-squared implied minimal chances of model overfitting. For warpage defect, the most significant parameters were packing pressure, melt temperature and cooling time while the most significant interactions involved the three parameters.

Table 7 shows the ANOVA results of shrinkage. ANOVA with main terms only yielded an R-squared of 96.27%, adjusted R-squared of 95.38% and predicted R-squared of 93.89% whereas ANOVA with interaction terms yielded an R-squared of 98.8%, adjusted R-squared of 97.94% and predicted R-squared of 96.21%. A significant interaction occurred between melt temperature and other less significant parameters such as mold temperature and injection pressure. Interaction effect sizes on shrinkage between the three parameters were found to be - 0.07, that between melt temperature and injection pressure -0.02, between mold temperature and injection pressure -0.01 and between melt temperature and mold temperature found to be - 0.002.

From the computed interaction effect sizes, the largest interaction effect occurred between melt temperature and injection pressure while the smallest effect occurred between melt temperature and mold temperature. Thus, considering the largest interaction effect among the three parameters occurred between melt temperature and injection pressure, the two parameters were selected over mold temperature.

Therefore, for the second stage design of experiment and predictive model development, five factors including melt temperature, injection pressure, packing time, packing pressure and cooling time were used as input variables.

Fig. 10 Contour plot showing the effect of packing pressure and packing time on shrinkage

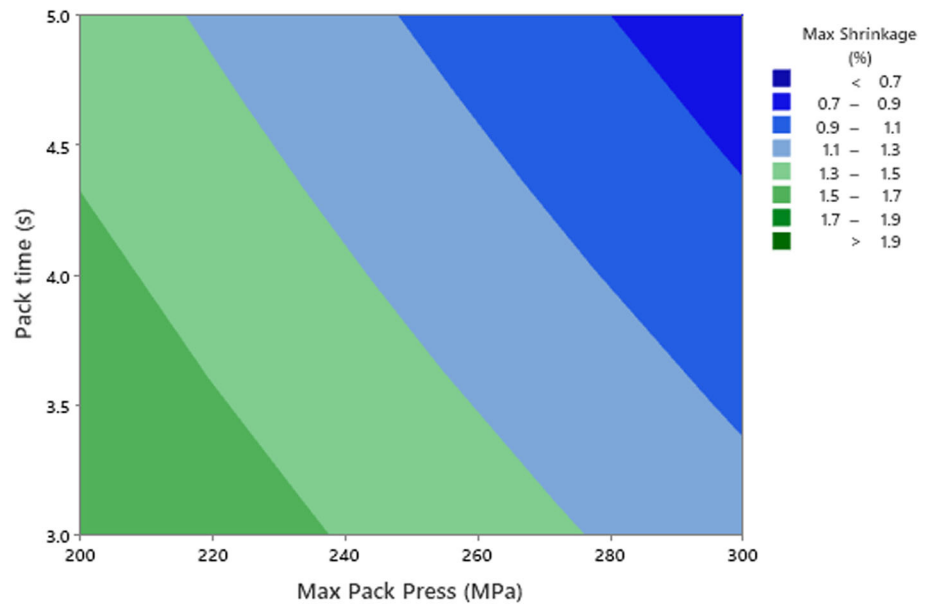
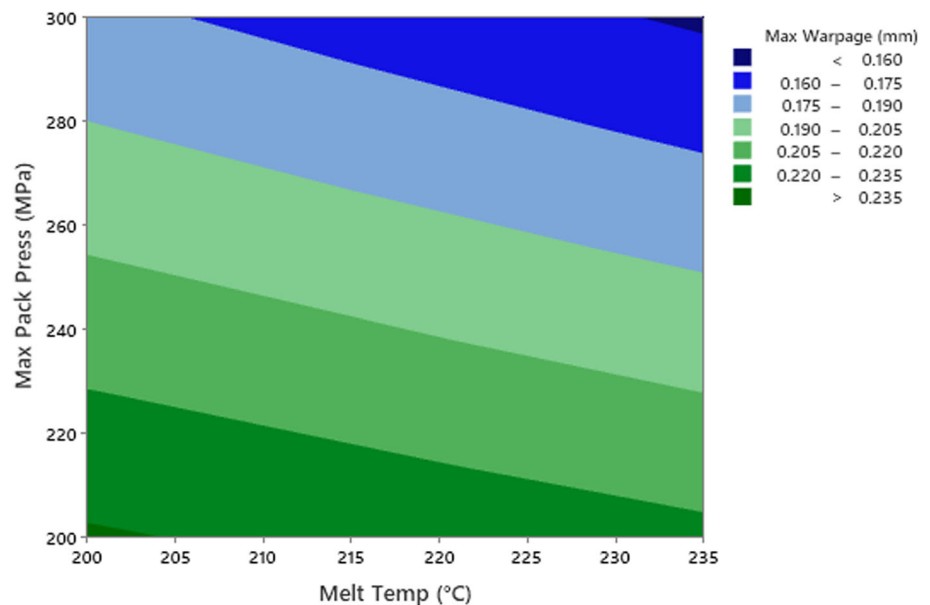


Fig. 11 Contour plot showing the effect of packing pressure and melt temperature on warpage



Taguchi experiment design

To enhance a more robust design and increase the predictive ability of the fuzzy inference model, five levels were used for each input parameter in the design of experiment stage. Table 8 shows the parameters used in the design with their levels of application.

Taguchi design was used for five input variables each at five levels and yielded an L25 orthogonal array. With the general objective of defect modelling being to minimize the defects, a smaller the better signal to noise ratio was calculated based on Eq. 16 (Altan, 2010).

$$SN = -10 \log \left[\frac{1}{n} \sum_{i=1}^n y_i^2 \right] \# \quad (16)$$

Table 9 shows the results of the numerical simulations. As carried out in the first DOE stage, the numerical data trend was validated against an experimental data trend obtained from a study by Mukras et al. (2019). Similar to the first DOE stage, a match in the trends was achieved. A general increase in melt temperature increased shrinkage whereas an increase in injection pressure, packing pressure, packing time and cooling time decreased shrinkage.

An additional simulation was carried out at different input levels that would be used for testing the performance and validation of the developed predictive models. Ten sets of input parameter combinations were randomly generated and used to perform numerical simulations. The distribution of the data was widened to accurately represent the problem

Table 6 ANOVA for warpage defect

Source	DF	Seq SS	Contribution	Adj MS	F-Value	P-Value
Melt Temp	1	2.3E-03	6.95%	2.3E-03	8243.15	0.000
Mold Temp	1	1.9E-07	0.00%	1.9E-07	0.66	0.426
Inj. Press	1	7.8E-11	0.00%	7.8E-11	0.00	0.987
Pack Time	1	1.9E-08	0.00%	1.9E-08	0.07	0.794
Pack Press	1	3.1E-02	92.68%	3.1E-02	109,952.48	0.000
Cool Time	1	1.6E-05	0.05%	1.6E-05	58.33	0.000
Melt Temp*Pack Press	1	9.8E-05	0.30%	9.8E-05	351.74	0.000
Melt Temp*Cool Time	1	3.7E-06	0.01%	3.7E-06	13.20	0.002
Inj. Press.*Pack Press	1	1.4E-09	0.00%	1.4E-09	0.00	0.945
Pack Time*Cool Time	1	1.5E-10	0.00%	1.5E-10	0.00	0.982
Error	21	5.9E-06	0.02%	2.8E-07		
Total	31	3.3E-02	100.00%			

Table 7 ANOVA for shrinkage defect

Source	DF	Seq SS	Contrib	Adj MS	F-value	P-value
Melt Temp	1	4.0E-02	0.86%	4.0E-02	12.88	0.002
Mold Temp	1	2.2E-04	0.00%	2.2E-04	0.07	0.795
Inj. Press	1	1.7E-03	0.04%	1.7E-03	0.55	0.466
Pack Time	1	9.8E-01	20.87%	9.8E-01	313.40	0.000
Pack Press	1	2.6E+00	55.83%	2.6E+00	838.62	0.000
Cool Time	1	8.8E-01	18.67%	8.8E-01	280.45	0.000
Melt Temp*Mold Temp	1	2.9E-05	0.00%	2.9E-05	0.01	0.925
Melt Temp*Inj. Press	1	2.4E-03	0.05%	2.4E-03	0.77	0.392
Melt Temp*Pack Press	1	3.0E-02	0.65%	3.0E-02	9.76	0.006
Mold Temp*Inj. Press	1	1.5E-03	0.03%	1.5E-03	0.47	0.503
Pack Time*Pack Press	1	2.2E-02	0.47%	2.2E-02	7.09	0.016
Pack Press.*Cool Time	1	1.6E-02	0.34%	1.6E-02	5.10	0.037
Melt Temp*Mold Temp*Inj. Press	1	4.6E-02	0.99%	4.6E-02	14.81	0.001
Error	18	5.6E-02	1.20%	3.1E-03		
Total	31	4.7E+00	100.00%			

Table 8 Selected model predictive process parameters with their levels of application

Parameter	Levels				
Melt temperature (°C)	200	210	220	230	240
Max. injection Pressure setting (MPa)	100	150	200	250	300
Max. packing Pressure setting (MPa)	100	150	200	250	300
Packing time (s)	2	3	4	5	6
Cooling time (s)	5	8	10	12	15

Table 9 Numerical simulation results based on Taguchi L25 design

Run	Melt Temp	Injection pressure	Pack pressure	Pack time	Cool time	Shrinkage (%)	Warpage (mm)	S/N ratio (dB)
1	200	100	100	2	5	2.76	0.283	- 5.853
2	200	150	150	3	8	2.33	0.266	- 4.393
3	200	200	200	4	10	1.38	0.237	0.086
4	200	250	250	5	12	1.18	0.209	1.439
5	200	300	300	6	15	0.36	0.178	10.934
6	210	100	150	4	12	1.95	0.264	- 2.869
7	210	150	200	5	15	1.25	0.231	0.926
8	210	200	250	6	5	1.51	0.202	- 0.646
9	210	250	300	2	8	1.45	0.170	- 0.276
10	210	300	100	3	10	2.21	0.279	- 3.946
11	220	100	200	6	8	1.48	0.229	- 0.498
12	220	150	250	2	10	1.62	0.200	- 1.246
13	220	200	300	3	12	1.13	0.167	1.855
14	220	250	100	4	15	1.92	0.280	- 2.747
15	220	300	150	5	5	2.39	0.255	- 4.607
16	230	100	250	3	15	1.25	0.198	0.964
17	230	150	300	4	5	1.47	0.157	- 0.385
18	230	200	100	5	8	2.56	0.280	- 5.206
19	230	250	150	6	10	1.70	0.253	- 1.694
20	230	300	200	2	12	2.16	0.226	- 3.726
21	240	100	300	5	10	0.84	0.157	4.376
22	240	150	100	6	12	2.20	0.278	- 3.907
23	240	200	150	2	15	2.00	0.252	- 3.079
24	240	250	200	3	5	2.37	0.221	- 4.522
25	240	300	250	4	8	1.49	0.191	- 0.524

Table 10 Model validation dataset

Run	Melt temperature	Injection pressure	Packing pressure	Packing time	Cooling time	Shrinkage (%)	Warpage (mm)
1	207	120	108	2	6	2.66	0.277
2	207	266	240	5	13	1.20	0.211
3	223	158	240	2	11	1.71	0.205
4	223	216	277	3	11	1.20	0.173
5	227	226	122	5	7	2.50	0.271
6	227	175	281	3	12	1.19	0.174
7	236	186	174	2	15	1.98	0.249
8	236	273	282	4	8	1.43	0.207
9	200	130	150	3	6	2.31	0.267
10	240	300	270	4	6	1.48	0.194

space and prevent further problems that would arise due to validation data set bias. Table 10 shows the results obtained from the numerical simulations of the validation data set.

Predictive model development

Fuzzy expert models were developed to predict the values of warpage and shrinkage defects at given process parameter inputs. Two Mamdani Fuzzy Inference Systems (FIS) were developed using MATLAB® Fuzzy Logic Designer and utilizing triangular and Gaussian membership function types. Triangular FIS was developed using triangular membership function types while Gaussian FIS developed based on Gaussian membership function types. The main components of the fuzzy logic predictive models developed were the fuzzifier, linguistic rule base, inference engine and defuzzifier.

Fuzzification

Through fuzzification, crisp input variables of five parameters namely melt temperature, injection pressure, packing pressure, packing time and cooling time were mapped onto fuzzy variables by expression as membership functions. Five membership functions were used for each of the five input variables. Linguistic labels chosen for each of the input membership functions were; Very Low (VL), Low (L), Medium (M), High (H) and Very High (VH). After trying different membership function types and their associated effects on the defect responses, triangular and Gaussian membership function types were deemed suitable and thus used in the fuzzification of the input variables. The degrees of membership in triangular and Gaussian membership functions were expressed as given in Eqs. 17 and 18 respectively (Lanzaro & Andrade, 2023).

$$f(x; a, b, c) = \begin{cases} 0, & x \leq a \\ \frac{x-a}{b-a}, & a \leq x \leq b \\ \frac{c-x}{c-b}, & b \leq x \leq c \\ 0, & c \leq x \end{cases} \quad (17)$$

$$f(x; \sigma, \mu) = e^{-\frac{(x-\mu)^2}{2\sigma^2}} \quad (18)$$

where a, b and c are the lower boundary, peak value and upper boundary of the membership class respectively and x is any arbitrary value between the lower and upper class boundary whose degree of membership is to be determined. For the Gaussian membership function, σ is the standard deviation of the membership class representing its width property, μ is the mean value of the membership class corresponding to the peak value while x is any arbitrary point whose membership value is to be determined.

Parameters of the membership functions were defined based on their levels given in Table 8. Figures 12 and 13 illustrates the triangular and Gaussian membership functions plots for one of the inputs (melt temperature) respectively.

Rule base formulation

A set of 25 IF-THEN rules governing the mapping of inputs into outputs were formulated through expert knowledge based on the 25 runs of data obtained from Taguchi based numerical simulations. The study assigned equal weights of 1 to each rule. The number of rules were maintained at 25 as repeated input combination trials revealed that the defined rules were the most likely to be fired for most input parameter combinations. Two of the rules are illustrated as follows;

IF (Melt Temperature is High) and (Injection Pressure is Medium) and (Packing Pressure is Very Low) and (Packing Time is High) and (Cooling Time is Low) THEN (Shrinkage is Very High), (Warpage is Very Very High)

IF (Melt Temperature is Very Low) and (Injection Pressure is Very High) and (Packing Pressure is Very High) and (Packing Time is Very High) and (Cooling Time is Very High) THEN (Shrinkage is Very Very Low), (Warpage is Very Low)

Defuzzification

To convert fuzzy variables back to crisp values, a centroid defuzzification method was used. This method calculated the center of area under the membership function and weighed the effect of each input variable towards the calculation. The study utilized ten membership functions for warpage and shrinkage responses. Figure 14 shows the symmetrically defined triangular membership function plots for shrinkage response.

Figure 15 shows Gaussian membership function plots for shrinkage response with 10 membership function classes. All the membership function classes are symmetrically placed, have a standard deviation of 0.1134 while the mean of each class is defined as the peak value of the given class.

Fuzzy inference system structure

Figure 16 illustrates a triangular membership function model structure with five inputs and two outputs and designed with triangular membership functions for input and output variables.

Parameter causality was easily identified from the rules interface of the developed models as illustrated in Fig. 17. It can be deduced from the interface that lower values of

Fig. 12 Triangular membership plot for melt temperature input values

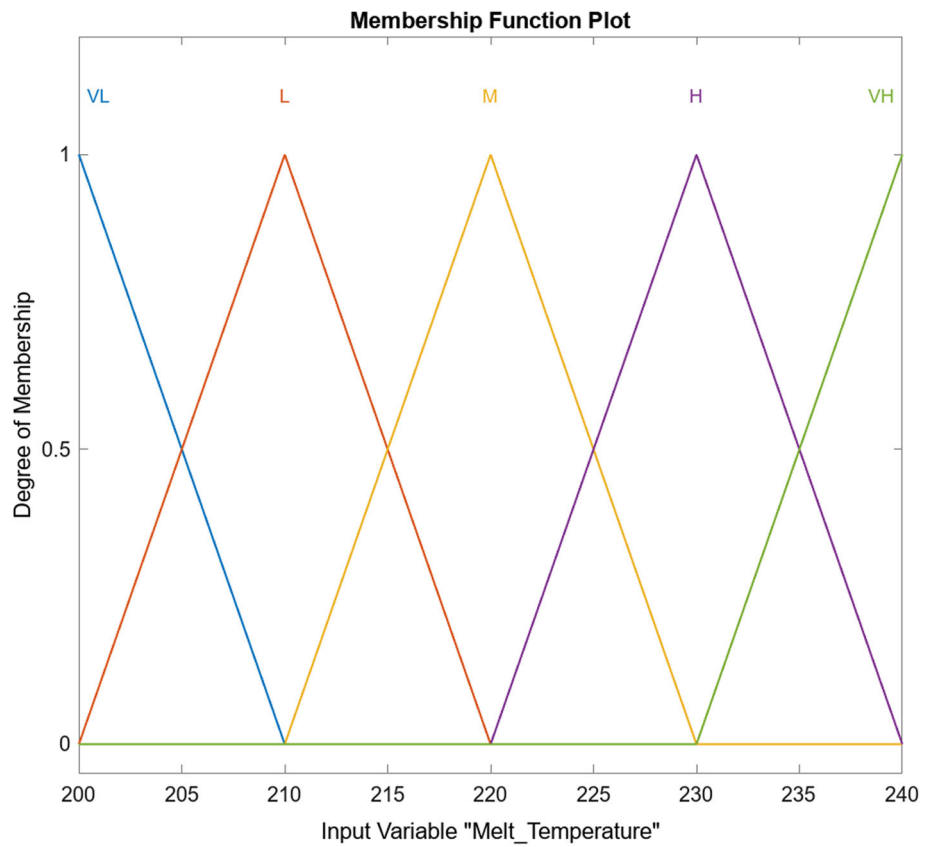


Fig. 13 Gaussian membership plot of melt temperature input values

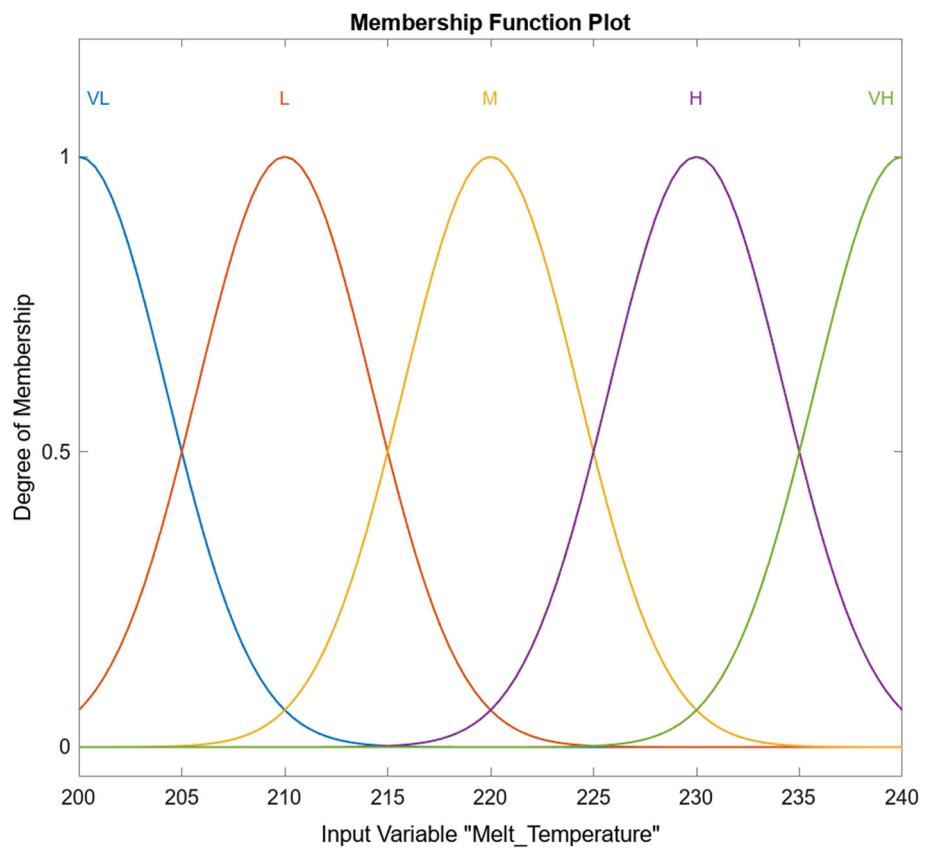


Fig. 14 Triangular membership functions for shrinkage response

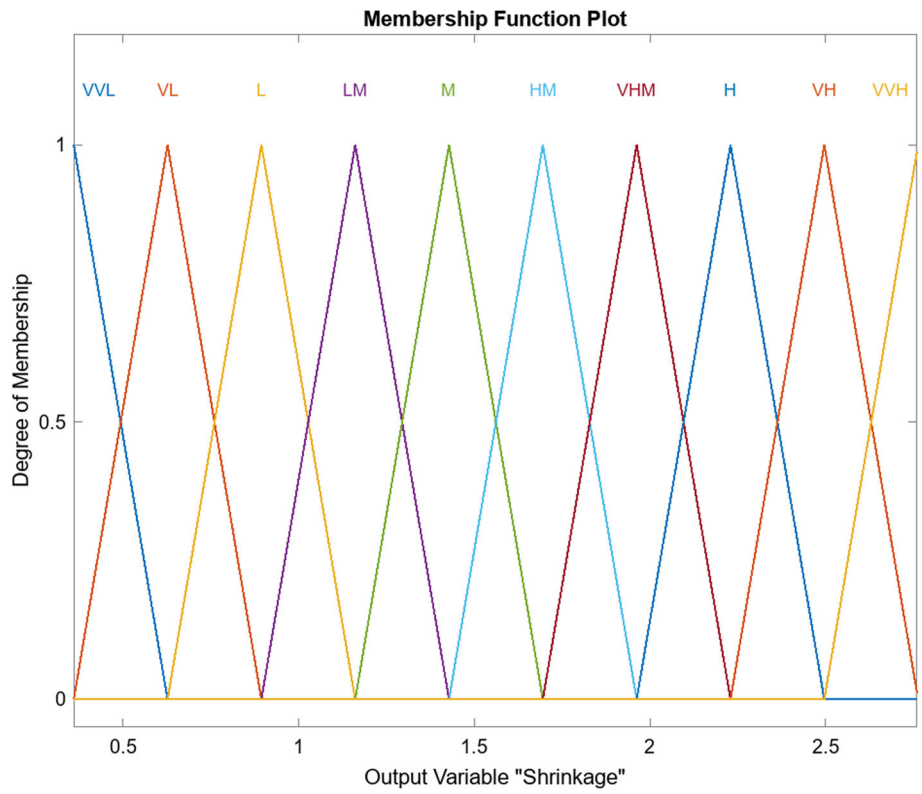


Fig. 15 Gaussian membership functions for shrinkage response

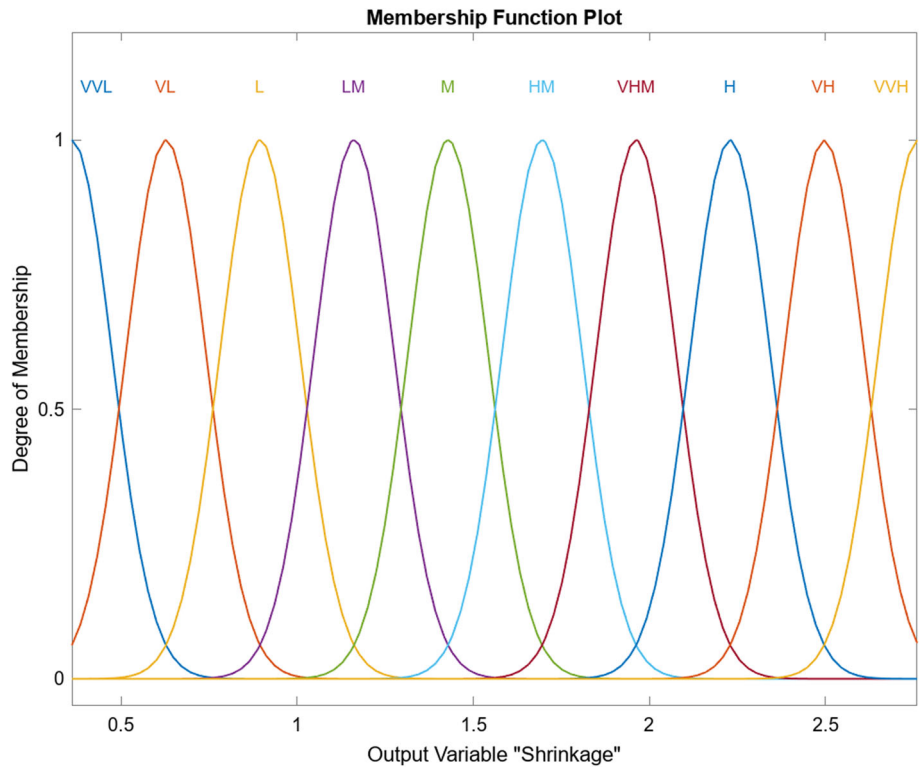


Fig. 16 Fuzzy Predictive Model based on triangular membership functions

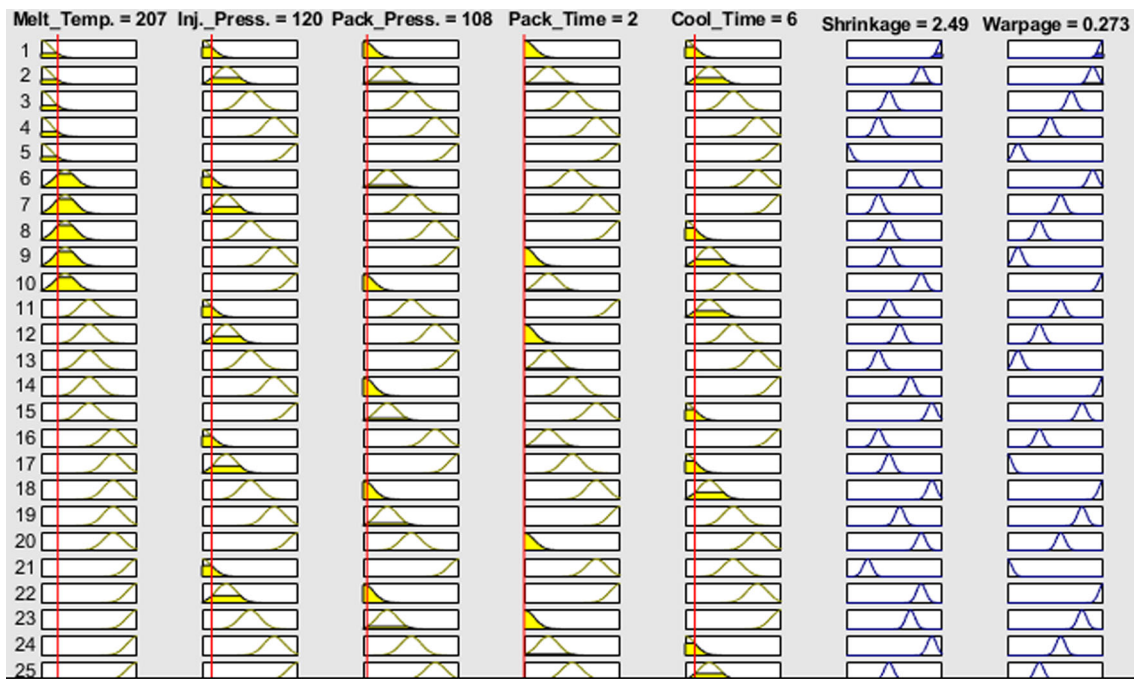
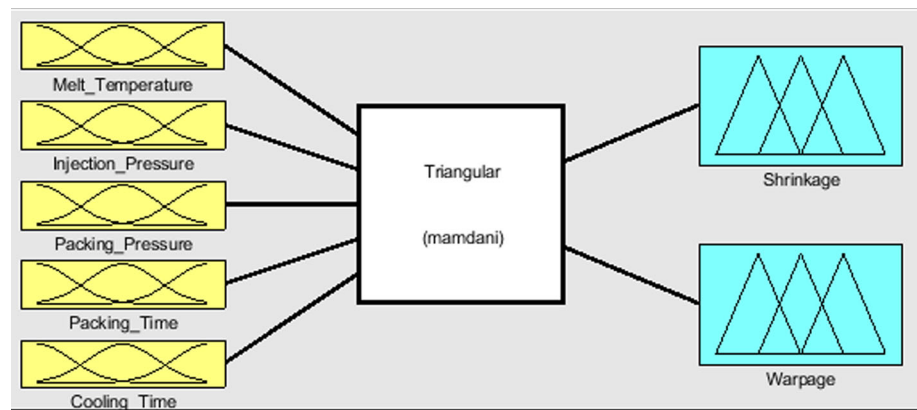


Fig. 17 Fuzzy predictive model rule base graphical interface

melt temperature are associated with lower values of shrinkage and higher values of warpage whereas lower values of packing pressure are associated with higher shrinkages and warpages.

Linguistic rule base representation from the FIS rule inference directly expresses the relationships among variables and hence facilitates an easy interpretation of how the model makes decisions. This transparency in prediction could form a basis for on-line injection molding process optimization.

Figure 18 illustrates a 3D surface plot from the developed FISs showing the relationship between packing pressure, melt temperature and warpage output. The smallest value of warpage was obtained at the highest values of melt temperature and packing pressure while the largest values of warpage were obtained at the lowest values of melt temperature and packing pressure. This relationship was similar

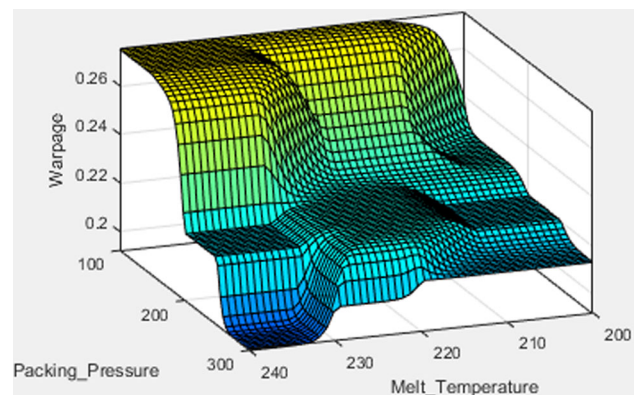
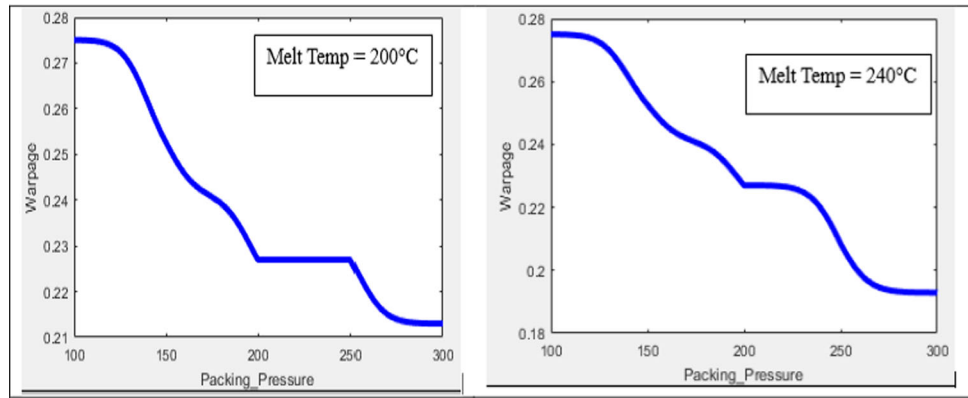


Fig. 18 FIS 3D surface plot on effect of melt temperature and packing pressure on warpage

Fig. 19 FIS 2D surface plot on effect of melt temperature and packing pressure on warpage



to that obtained statistically during factorial analysis illustrated in Fig. 11. 2D plots at two levels of melt temperature were made as illustrated in Fig. 19. At a melt temperature of 200 °C, increasing the maximum packing pressure setting from 100 to 300 MPa decreased the warpage from 0.275 to 0.212 whereas, at a melt temperature of 240 °C, a similar increase in packing pressure decreased the warpage from 0.277 to 0.190. This illustrated that the developed FIS models captured the interaction effects between the process parameters.

Model tuning and validation

This study determined the parameters of the fuzzy model membership functions through intuition and further carried out tuning of the parameters using a pattern search optimization technique (Tremante et al., 2019). As a local optimization technique, the pattern search algorithm does well for models with smaller parameter tuning ranges in comparison to global optimization algorithms which do well for large parameter tuning ranges. Tuning of fuzzy model parameters was carried out based on the data set of the simulation results used for rule formulation. The tuning was based on a default cost function obtained as the root mean square error between the actual outputs and the initial fuzzy predicted outputs.

The convergence criteria used for the tuning was the distance metric (RMSE) of data sets in Table 9 used for the development of fuzzy inference systems. The objective function $f(x)$ to be minimized was calculated for each FIS based on the differences between the reference outputs obtained from simulations and FIS-predicted outputs. For twenty-five data sets and two outputs, $f(x)$ was calculated using Eq. 19 (Ross, 2010).

$$f(x) = \sqrt{\frac{1}{25} \sum_{i=1}^{25} ((y_{1i,ref} - y_{1i,pred})^2 + (y_{2i,ref} - y_{2i,pred})^2)} \tag{19}$$

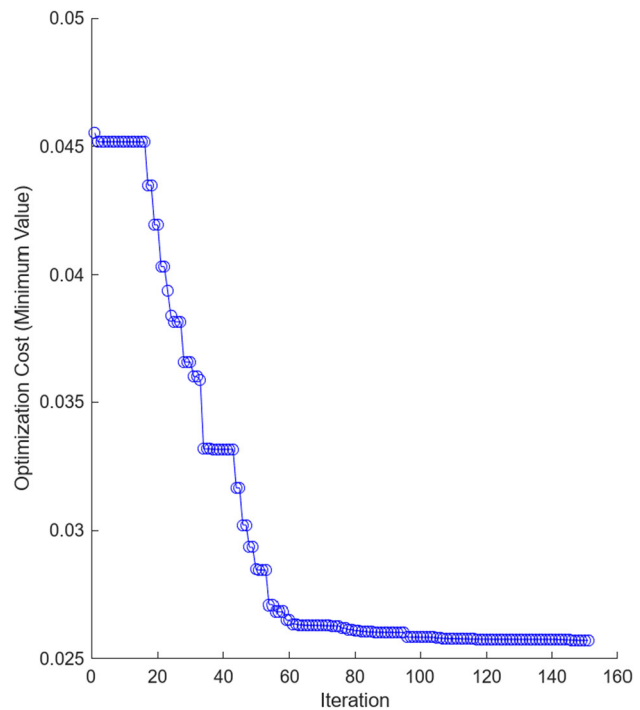


Fig. 20 Triangular FIS tuning convergence result showing a convergence plot

where $y_{1i,ref}$ is the reference shrinkage output for the i^{th} data point, $y_{1i,pred}$ is the predicted shrinkage output for the i^{th} data point, $y_{2i,ref}$ is the reference warpage output for the i^{th} data point and $y_{2i,pred}$ is the predicted warpage output for the i^{th} data point.

With the objective function in place, the optimization algorithm iteratively adjusts the various fuzzy inference system parameters such as input membership function parameters, output membership function parameters and rules until the objective function converges to a minimum solution. Figure 20 shows the tuning convergence plot for a fuzzy inference system with a triangular membership function type. Convergence was achieved after 150 iterations with the objective function reducing from 0.0464 to 0.0257. Mesh

sizes of up to 0.0078 were utilized indicating a finer exploration of the search space.

The resulting tuned triangular FIS had adjusted rule weights whereas the input and output membership function parameters were unchanged. Upon successful tuning, the performances of the initially designed triangular FIS and tuned FIS were tested against a validation data set given in Table 10. Using the outputs from the validation data set as the reference outputs, the RMSE for both the initial FIS and tuned FIS were obtained. Figures 21 and 22 show the comparison of prediction results and errors for shrinkage (Output 1) and warpage (Output 2) responses. Reference curve represents the validation set of results obtained from numerical simulation. The tuned FIS has a slightly lower RMSE compared to the initial FIS for both the shrinkage and warpage outputs. The prediction errors were reduced from 0.036 to 0.03 for shrinkage prediction and 0.0045 to 0.0044 for warpage prediction. Through tuning, the search algorithm captured underlying relationships in the data and modified given rule weightings to better reflect the data patterns thereby reducing model prediction errors and enhancing accuracy (Nikolić et al., 2020). Such accuracies could also be obtained by machine learning through boosting ensemble (Bustillo et al., 2018). The prediction error plots indicate that the shrinkage response was over-predicted for most instances whereas the warpage response was under-predicted for most instances.

Similarly, the Gaussian membership function-based FIS inputs, rules and output membership functions were tuned using a pattern search algorithm. A convergence was achieved after 100 iterations with the objective function reducing from 0.066 to 0.033. A mesh size of up to 0.5 was used indicating a finer exploration of the search space.

Tuning of the Gaussian FIS adjusted various individual rule weightings but did not adjust the input and output membership function parameters indicating an optimal specification of input and output membership function parameters in the initial design. Figures 23 and 24 show the comparison of prediction results and errors obtained for the initial and tuned Gaussian-based FIS. Reference curve represents the values obtained from numerical simulation. By tuning, the RMSE for shrinkage was reduced from 0.073 to 0.065 as shown in Fig. 23 while the RMSE for warpage slightly increased from 0.005 to 0.006 as shown in Fig. 24 suggesting that the optimization process had a differential impact on the two responses.

In addition to the RMSE, a coefficient of determination and standard error of regression were determined for the four FISs to assess the abilities of the models to predict the outcomes in a linear regression setting. The coefficient of determination and standard error of regression were calculated at a 95% confidence level. As a result of the possible non-linearity of the plastic injection molding process, this study used standard error of regression metric to evaluate the

performance of the predictive model alongside the coefficient of determination metric.

Table 11 shows the performance metrics of the four predictive models computed for each output variable prediction. The tuned triangular FIS had the lowest RMSE for both the outputs which indicated a good predictive capability. It also had the lowest standard error of regression on warpage and the highest coefficient of determination on warpage prediction. A tuned Gaussian FIS had higher values of RMSE but performed better in terms of model fitting as given by standard error of regression and coefficient of determination performance metrics. The generally good performance of the FIS models on the validation data set was an indication of minimal chances of model overfitting to the training data set.

Therefore, for shrinkage and warpage defects predictive modelling in plastic injection molding, a tuned FIS with triangular membership functions would be recommended. This model had RMSEs of 0.03 and 0.004, standard errors of regression of 8.75 and 1.19 and coefficients of determination of 98.9% and 96.5% for shrinkage and warpage prediction respectively. These performance metrics such as coefficient of determination (R^2) compared well with those of other predictive models based on other strategies reported in literature as summarized in Table 12.

Conclusions

The following conclusions were made from this study;

1. Consideration of process parameter interactions as well as parameter main effects in the parameter screening stage enhances a more robust and accurate predictive model development. Interactions account for the combined effects of variables and thereby allowing the model to capture how the individual effects of a certain parameter depend on the levels of application of the other parameters. Consideration of parameter interactions necessitated the inclusion of injection pressure which would otherwise not have been selected had the screening been based on the main effect only.
2. In warpage and shrinkage modelling, the most significant process parameter influencing the defects is packing pressure setting while the most significant process parameter interactions influencing the defects involve the melt temperature. Packing pressure contributes to warpage defect by 92% and to shrinkage defect by 55%.
3. Despite shrinkage being one of the causes of warpage defect, the degree of effects of process parameters on the two defects vary. A given change in process parameters could induce a decreasing effect on shrinkage while increasing warpage and vice versa. An increase in melt temperature reduced warpage but increased

Fig. 21 Triangular FIS shrinkage prediction errors

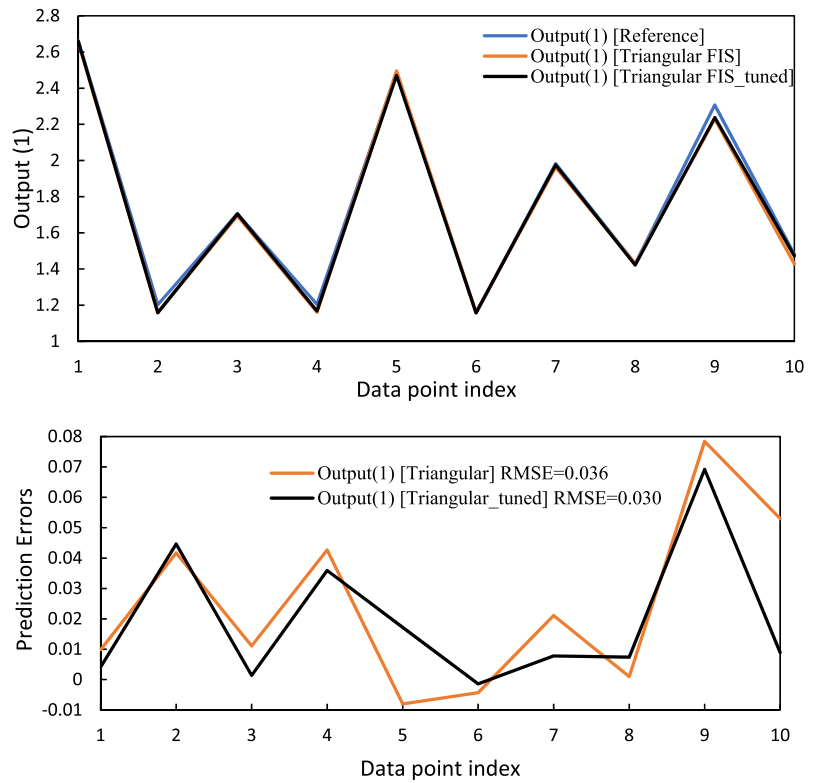


Fig. 22 Triangular FIS warpage prediction errors

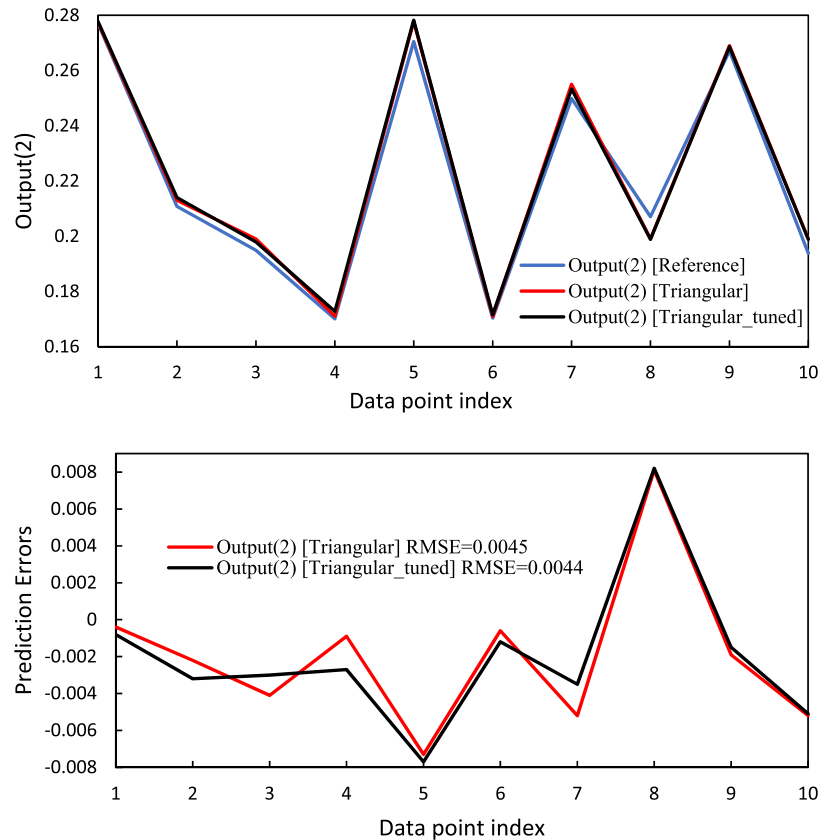


Fig. 23 Gaussian FIS shrinkage prediction errors

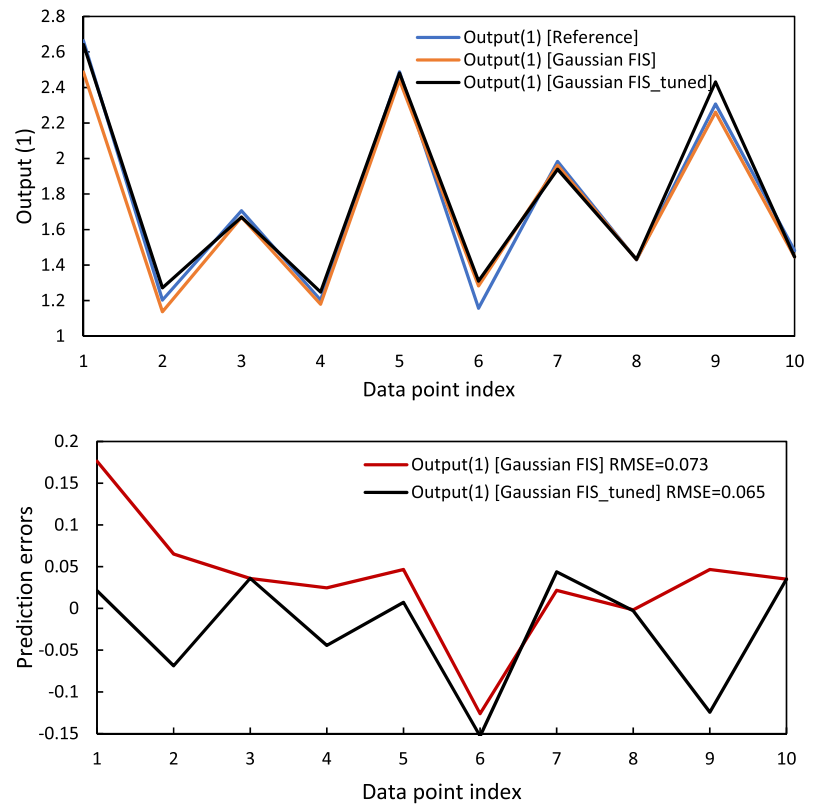


Fig. 24 Gaussian FIS warpage prediction errors

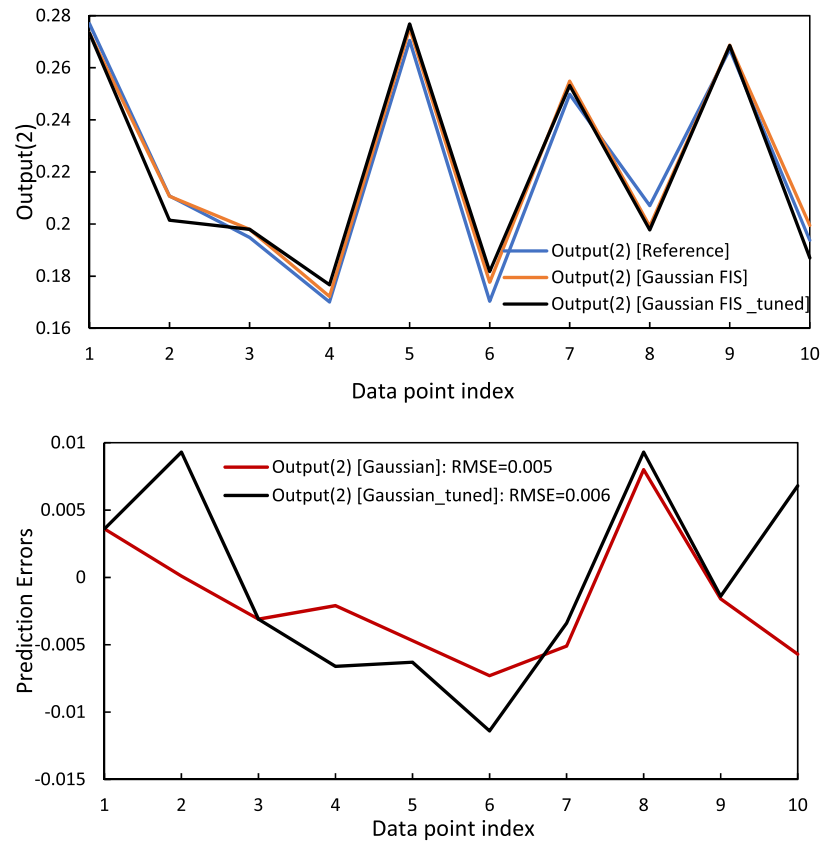


Table 11 Performance metrics of the developed FISs

Membership function	Performance metric					
	Root mean square error (RMSE)		Standard error of regression (S) (%)		Coefficient of determination (R ²) (%)	
	Shrinkage	Warpage	Shrinkage	Warpage	Shrinkage	Warpage
Triangular	0.037	0.005	9.63	1.24	98.71	96.25
Triangular tuned	0.030	0.004	8.75	1.19	98.93	96.48
Gaussian	0.073	0.005	8.04	1.29	98.94	95.52
Gaussian tuned	0.065	0.006	6.55	1.20	99.36	96.20

Table 12 Model performance metrics reported from similar studies

Study	Model	Response	CoD (R ²)
Abdul et al. (2019)	ANN	Shrinkage	91%
Tsai and Luo (2017)	ANN + GA	Dimension accuracy	96.75%
Chen et al. (2020)	ANN	Dimensional variation	91%
Hidayah et al. (2018)	GA + RSM	Warpage	98.1%
Kumar et al. (2020)	PSO + Regression	Shrinkage Warpage	94.1% 92.4%
Chen et al., (2023a, 2023b)	ANN + MLR	Dimensional stability	99.8%
Ahmed et al. (2022)	Random forest algorithm	Warpage	96.75%
	Gradient boosted regression	Warpage	90.63%
Proposed method in this study	Triangular FIS model	Shrinkage	98.93%
	Gaussian FIS model	Shrinkage	99.36%
	Triangular FIS model	Warpage	96.48%
	Gaussian FIS model	Warpage	96.20%

shrinkage. Similarly, changes in mold temperature, injection pressure and cooling time had opposing effects on the two defects. Therefore, optimization and predictive modelling of the two defects should be carried out concurrently.

- An integrated fuzzy logic rule base system with a pattern search algorithm compares well with other models for predictive modelling of shrinkage and warpage defects. Tuning of all the developed models through pattern

search lowered the models' standard error of regression and RMSE and increased the coefficient of determination. For triangular FIS shrinkage prediction, tuning lowered the model RMSE from 0.037 to 0.030, lowered the model standard error of regression from 9.63 to 8.75 and increased the model coefficient of determination from 98.71% to 98.93%. Tuning of expert-designed fuzzy inference systems using intelligent algorithms helps to improve the predictive ability of the models resulting in enhanced performance.

- Both triangular and Gaussian membership functions accurately model shrinkage and warpage defects in the plastic injection molding process. The triangular membership function model had lower values of RMSE indicating a higher predictive accuracy whereas the Gaussian membership function model had lower values of the standard error of regression indicating higher model reliability. For shrinkage prediction, triangular FIS had an RMSE of 0.03 and a standard error of regression of 8.75 whereas Gaussian FIS had an RMSE of 0.06 and a standard error of regression of 6.25.

Author contributions Conceptualization, analysis and investigation: [Steven Otieno, Edwell Mharakurwa, Fredrick Mwema]; writing—original draft preparation: [Steven Otieno, Job Wambua]; writing—review and editing: [Edwell Mharakurwa, Fredrick Mwema, Tien-Chien Jen, Esther Akinlabi]; supervision: [Esther Akinlabi, Tien-Chien Jen].

Funding This research received no external funding.

Data availability This study presents all data adopted during the research.

Declarations

Conflict of interest There are no known conflicts of interests declared on methods and results obtained in this study.

Consent for publication All authors consent to publishing of results from the study.

References

- Abasalizadeh, M., Hasanzadeh, R., Mohamadian, Z., Azdast, T., & Rostami, M. (2018). Experimental study to optimize shrinkage behavior of semi-crystalline and amorphous thermoplastics. *Iranian Journal of Materials Science & Engineering*, 15(4), 41–51. <https://doi.org/10.22068/ijmse.15.4.41>
- Abdul, R., Guo, G., Chen, J. C., Jung, J., & Yoo, W. (2019). Shrinkage prediction of injection molded high density polyethylene parts with taguchi/artificial neural network hybrid experimental design. *International Journal on Interactive Design and Manufacturing*. <https://doi.org/10.1007/s12008-019-00593-4>
- Ahmed, T., Sharma, P., Karmaker, C. L., & Nasir, S. (2022). Warpage prediction of injection-molded PVC part using ensemble machine learning algorithm. *Materials Today: Proceedings*, 50, 565–569. <https://doi.org/10.1016/J.MATPR.2020.11.463>
- Ai, Y., Han, S., Lei, C., & Cheng, J. (2023a). The characteristics extraction of weld seam in the laser welding of dissimilar materials by different image segmentation methods. *Optics and Laser Technology*, 167, 109740. <https://doi.org/10.1016/j.optlastec.2023.10.9740>
- Ai, Y., Yan, Y., Dong, G., & Han, S. (2023b). Investigation of microstructure evolution process in circular shaped oscillating laser welding of Inconel 718 superalloy. *International Journal of Heat and Mass Transfer*, 216, 124522. <https://doi.org/10.1016/j.ijheatmasstransfer.2023.124522>
- Altan, M. (2010). Reducing shrinkage in injection moldings via the Taguchi, ANOVA and neural network methods. *Materials & Design*, 31(1), 599–604. <https://doi.org/10.1016/J.MATDES.2009.06.049>
- Bustillo, A., Urbikain, G., Perez, J. M., Pereira, O. M., & Lopez de Lacalle, L. N. (2018). Smart optimization of a friction-drilling process based on boosting ensembles. *Journal of Manufacturing Systems*, 48, 108–121. <https://doi.org/10.1016/j.jmsy.2018.06.004>
- Chang, R., Chen, C., & Su, K. (1996). Modifying the tait equation with cooling-rate effects to predict the pressure–volume–temperature behaviors of amorphous polymers: Modeling and experiments. *Polymer Engineering & Science*, 36(13), 1789–1795. <https://doi.org/10.1002/pen.10574>
- Chen, J., Cui, Y., Liu, Y., & Cui, J. (2023b). Design and parametric optimization of the injection molding process using statistical analysis and numerical simulation. *Processes*, 11(414), 1–17. <https://doi.org/10.3390/pr11020414>
- Chen, J. C., Guo, G., & Chang, Y. H. (2023a). Intelligent dimensional prediction systems with real-time monitoring sensors for injection molding via statistical regression and artificial neural networks. *International Journal on Interactive Design and Manufacturing*, 17(3), 1265–1276. <https://doi.org/10.1007/s12008-022-01115-5>
- Chen, J. C., Guo, G., & Wang, W. N. (2020). Artificial neural network-based online defect detection system with in-mold temperature and pressure sensors for high precision injection molding. *The International Journal of Advanced Manufacturing Technology*, 110(7–8), 2023–2033. <https://doi.org/10.1007/s00170-020-06011-4>
- Chen, Y., & Zhu, J. (2019). Warpage analysis and optimization of thin-walled injection molding parts based on numerical simulation and orthogonal experiment. *IOP Conference Series: Materials Science and Engineering*. <https://doi.org/10.1088/1757-899X/688/3/033027>
- Chen, Z., & Turng, L. S. (2005). A review of current developments in process and quality control for injection molding. *Advances in Polymer Technology*, 24(3), 165–182. <https://doi.org/10.1002/adv.20046>
- Fischer, J. M. (2013). Causes of molded part variation: Processing. *Handbook of molded part shrinkage and warpage* (3rd ed., pp. 81–100). William Andrew. <https://doi.org/10.1016/b978-1-4557-2597-7.00001-x>
- Fu, J., & Ma, Y. (2016). Mold modification methods to fix warpage problems for plastic molding products. *Computer-Aided Design and Applications*, 13(1), 138–151. <https://doi.org/10.1080/16864360.2015.1059203>
- Gao, Y., & Wang, X. (2008). An effective warpage optimization method in injection molding based on the Kriging model. *The International Journal of Advanced Manufacturing Technology*, 37(9), 953–960. <https://doi.org/10.1007/s00170-007-1044-6>
- Hidayah, M. H. N., Shayfull, Z., Noriman, N. Z., Fathullah, M., Norshahira, R., & Miza, A. T. N. A. (2018). Optimization of warpage on plastic part by using genetic algorithm (GA). *AIP Conference Proceedings*. <https://doi.org/10.1063/1.5066804>
- Hu, Y., & Wu, K. (2022). Application of expert adjustable fuzzy control algorithm in temperature control system of injection machines. *Computational Intelligence and Neuroscience*. <https://doi.org/10.1155/2022/3616814>
- Huszar, M., Belblidia, F., Davies, H. M., Arnold, C., Bould, D., & Sienz, J. (2015). Sustainable injection moulding: The impact of materials selection and gate location on part warpage and injection pressure. *Sustainable Materials and Technologies*, 5, 1–8. <https://doi.org/10.1016/j.susmat.2015.07.001>
- Kennedy, P., & Zheng, R. (2013). *Flow analysis of injection molds* (2nd ed.). Hanser Publications. <https://doi.org/10.3139/9781569905227>
- Khosravani, M. R., & Nasiri, S. (2020). Injection molding manufacturing process: Review of case-based reasoning applications. *Journal of Intelligent Manufacturing*, 31(4), 847–864. <https://doi.org/10.1007/s10845-019-01481-0>
- Kumar, S., Singh, A. K., & Pathak, V. K. (2020). Modelling and optimization of injection molding process for PBT/PET parts using modified particle swarm algorithm. *Indian Journal of Engineering and Materials Sciences*, 27(3), 603–615. <https://doi.org/10.56042/ijems.v27i3.45057>
- Lanzaro, G., & Andrade, M. (2023). A fuzzy expert system for setting Brazilian highway speed limits. *International Journal of Transportation Science and Technology*, 12(2), 505–524. <https://doi.org/10.1016/J.IJTST.2022.05.003>
- Li, K., Yan, S., Zhong, Y., Pan, W., & Zhao, G. (2019). Multi-objective optimization of the fiber-reinforced composite injection molding process using Taguchi method, RSM, and NSGA-II. *Simulation Modelling Practice and Theory*, 91, 69–82. <https://doi.org/10.1016/j.simpat.2018.09.003>
- Lin, W. C., Fan, F. Y., Huang, C. F., Shen, Y. K., & Wang, H. (2022). Analysis of the warpage phenomenon of micro-sized parts with precision injection molding by experiment, numerical simulation, and grey theory. *Polymers*. <https://doi.org/10.3390/polym14091845>
- López De Lacalle, L. N., Lamikiz, A., Muñoa, J., & Sánchez, J. A. (2005). The CAM as the centre of gravity of the five-axis high speed milling of complex parts. *International Journal of Production Research*, 43(10), 1983–1999. <https://doi.org/10.1080/00207540412331330129>
- Mieth, F., & Tromm, M. (2016). Multicomponent technologies. *Specialized injection molding techniques* (pp. 1–51). William Andrew Publishing. <https://doi.org/10.1016/B978-0-323-34100-4.00001-8>
- Moayyedean, M., Abhary, K., & Marian, R. (2018). Optimization of injection molding process based on fuzzy quality evaluation and Taguchi experimental design. *CIRP Journal of Manufacturing Science and Technology*, 21, 150–160. <https://doi.org/10.1016/J.CIRPJ.2017.12.001>
- Mohan, M., Ansari, M. N. M., & Shanks, R. A. (2017). Review on the effects of process parameters on strength, shrinkage, and warpage

- of injection molding plastic component. *Polymer - Plastics Technology and Engineering*, 56(1), 1–12. <https://doi.org/10.1080/03602559.2015.1132466>
- Mukras, S. M. S., Omar, H. M., & Al-Mufadi, F. A. (2019). Experimental-based multi-objective optimization of injection molding process parameters. *Arabian Journal for Science and Engineering*, 44(9), 7653–7665. <https://doi.org/10.1007/s13369-019-03855-1>
- Nikolić, M., Šelmić, M., Macura, D., & Čalić, J. (2020). Bee colony optimization metaheuristic for fuzzy membership functions tuning. *Expert Systems with Applications*, 158, 1–10. <https://doi.org/10.1016/j.eswa.2020.113601>
- Packianather, M., Chan, F., Griffiths, C., Dimov, S., & Pham, D. T. (2013). Optimisation of micro injection moulding process through design of experiments. *Procedia CIRP*, 12, 300–305. <https://doi.org/10.1016/j.PROCIR.2013.09.052>
- Phoa, F. K. H., Wong, W. K., & Xu, H. (2009). The need of considering the interactions in the analysis of screening designs. *Journal of Chemometrics*, 23(10), 545–553. <https://doi.org/10.1002/CEM.1252>
- Rosato, D. V., & Rosato, M. G. (2012). Injection molding handbook. *Springer Science & Business Media*. <https://doi.org/10.1007/978-1-4615-4597-2>
- Ross, T. J. (2010). *Fuzzy logic with engineering applications* (3rd ed.). New York: Wiley. <https://doi.org/10.1002/9781119994374>
- Silva, B., Marques, R., Faustino, D., Ilheu, P., Santos, T., Sousa, J., & Rocha, A. D. (2023). Enhance the injection molding quality prediction with artificial intelligence to reach zero-defect manufacturing. *Processes*, 11(1), 62. <https://doi.org/10.3390/pr11010062>
- Song, Z., Liu, S., Wang, X., & Hu, Z. (2020). Optimization and prediction of volume shrinkage and warpage of injection-molded thin-walled parts based on neural network. *The International Journal of Advanced Manufacturing Technology*, 109(3–4), 755–769. <https://doi.org/10.1007/s00170-020-05558-6>
- Tremante, P., Yen, K., & Brea, E. (2019). Tuning of the membership functions of a fuzzy control system using pattern search optimization method. *Journal of Intelligent and Fuzzy Systems*, 37(3), 3763–3776. <https://doi.org/10.3233/JIFS-190003>
- Tsai, K. M., & Luo, H. J. (2017). An inverse model for injection molding of optical lens using artificial neural network coupled with genetic algorithm. *Journal of Intelligent Manufacturing*, 28(2), 473–487. <https://doi.org/10.1007/s10845-014-0999-z>
- Wang, X., Gu, J., Shen, C., & Wang, X. (2015). Warpage optimization with dynamic injection molding technology and sequential optimization method. *International Journal of Advanced Manufacturing Technology*, 78(1–4), 177–187. <https://doi.org/10.1007/s00170-014-6621-x>
- Yang, K., Tang, L., & Wu, P. (2022). Research on optimization of injection molding process parameters of automobile plastic front-end frame. *Advances in Materials Science and Engineering*, 2022, 1–18. <https://doi.org/10.1155/2022/5955725>
- Yang, W. H., Peng, A., Liu, L., Hsu, D. C., & Chang, R. Y. (2004). Integrated numerical simulation of injection molding using true 3D approach. *Annual Technical Conference - ANTEC, Conference Proceedings, 1*, 486–490.
- Yin, F., Mao, H., Hua, L., Guo, W., & Shu, M. (2011). Back Propagation neural network modeling for warpage prediction and optimization of plastic products during injection molding. *Materials & Design*, 32(4), 1844–1850. <https://doi.org/10.1016/J.MATDES.2010.12.022>
- Yu, S., Zhang, T., Zhang, Y., Huang, Z., Gao, H., Han, W., Turng, L. S., & Zhou, H. (2022). Intelligent setting of process parameters for injection molding based on case-based reasoning of molding features. *Journal of Intelligent Manufacturing*, 33(1), 77–89. <https://doi.org/10.1007/s10845-020-01658-y>
- Zhang, H., Fang, F., Gilchrist, M. D., & Zhang, N. (2019). Precision replication of micro features using micro injection moulding: Process simulation and validation. *Materials and Design*, 177(9), 107829. <https://doi.org/10.1016/j.matdes.2019.107829>
- Zhao, N. Y., Lian, J. Y., Wang, P. F., & Xu, Z. Bin. (2022). Recent progress in minimizing the warpage and shrinkage deformations by the optimization of process parameters in plastic injection molding: A review. *International Journal of Advanced Manufacturing Technology*, 120(1–2), 85–101. <https://doi.org/10.1007/s00170-022-08859-0>
- Zhou, H. (2013). *Computer modeling for injection molding: Simulation, optimization, and control* (1st ed.). Wiley.

Publisher's Note Springer Nature remains neutral with regard to jurisdictional claims in published maps and institutional affiliations.

Springer Nature or its licensor (e.g. a society or other partner) holds exclusive rights to this article under a publishing agreement with the author(s) or other rightsholder(s); author self-archiving of the accepted manuscript version of this article is solely governed by the terms of such publishing agreement and applicable law.